PETROGRAPHY AND DIAGENESIS OF THE TRAVIS PEAK (HOSSTON) FORMATION, EAST TEXAS

TOPICAL REPORT
(February-September 1985)

Prepared by

Shirley P. Dutton

Assisted by

Patricia Bobeck

Bureau of Economic Geology
W. L. Fisher, Director
The University of Texas at Austin
Austin, Texas 78713

Prepared for

The Gas Research Institute
Contract No. 5082-211-0708
Scot C. Hathaway, GRI Project Manager

September 1985

DISCLAIMER

LEGAL NOTICE This report was prepared by the Bureau of Economic Geology as an account of work sponsored by the Gas Research Institute (GRI). Neither GRI, members of GRI, nor any person acting on behalf of either:

a. Makes any warranty or representation, express or implied, with respect to the accuracy, completeness, or usefulness of the information contained in this report, or that the use of any apparatus, method, or process disclosed in this report may not infringe privately owned rights; or

b. Assumes any liability with respect to the use of, or for damages resulting from the use of, any information, apparatus, method, or process disclosed in this report.

50272-101

REPORT DOCUMENTATION PAGE	1. REPORT NO. GRI-85/0220	2.	3. Recipient's Accession No.

4. Title and Subtitle
Petrography and Diagenesis of the Travis Peak (Hosston) Formation, East Texas

5. Report Date
September 30, 1985

6.

7. Author(s)
Shirley P. Dutton

8. Performing Organization Rept. No.

9. Performing Organization Name and Address
Bureau of Economic Geology
The University of Texas at Austin
University Station, Box X
Austin, Texas 78713

10. Project/Task/Work Unit No.

11. Contract(C) or Grant(G) No.
(C) 5082-211-0708
(G) (Gas Research Institute)

12. Sponsoring Organization Name and Address
Gas Research Institute
8600 West Bryn Mawr Ave.
Chicago, Illinois 60631

Project Manager:
Scot C. Hathaway

13. Type of Report & Period Covered
Research
Feb. 1985 - Sept. 1985

14.

15. Supplementary Notes

16. Abstract (Limit: 200 words)

Petrographic studies of the Travis Peak Formation in East Texas were used to interpret the diagenetic history of Travis Peak sandstones and to relate the diagenetic history to permeability variations within the formation.

Travis Peak sandstones are fine to very fine grained quartzarenites and subarkoses that were derived from sedimentary, metamorphic, and igneous rocks exposed in a large area of the southwestern United States. The originally high depositional porosity in matrix-free sandstones was reduced by compaction and precipitation of authigenic cements, particularly quartz, ankerite, illite, and chlorite. In addition, reservoir bitumen, a high molecular weight hydrocarbon residue, occludes porosity in some zones near the top of the Travis Peak. Porosity and permeability have a wide range of values at the top of the formation, but both the range of values and the maximum values decrease with depth below the top of the Travis Peak. Dissolution of orthoclase and plagioclase has formed most of the secondary porosity. Porosimeter-measured porosity is the best predictor of permeability, and there is a significant inverse correlation between total volume of cement and permeability.

17. Document Analysis a. Descriptors
East Texas, Hosston Formation, sandstone diagenesis, tight gas sandstones, Travis Peak Formation

b. Identifiers/Open-Ended Terms
petrography of Travis Peak Formation, diagenetic history of tight gas sandstones

c. COSATI Field/Group

18. Availability Statement	19. Security Class (This Report)	21. No. of Pages
Release unlimited	unclassified	84
	20. Security Class (This Page) unclassified	22. Price

(See ANSI-Z39.18) See Instructions on Reverse

OPTIONAL FORM 272 (4-77)
(Formerly NTIS-35)
Department of Commerce

RESEARCH SUMMARY

Title	Petrography and Diagenesis of the Travis Peak (Hosston) Formation, East Texas
Contractor	Bureau of Economic Geology, The University of Texas at Austin, GRI Contract No. 5082-211-0708, entitled "Geologic Analysis of Travis Peak/Hosston and Corcoran-Cozzette Tight Gas Sandstones."
Principal Investigator	R. J. Finley
Report Period	February-September 1985 Topical Report
Objective	To present the results of petrographic studies of the Travis Peak Formation in East Texas based on data from 10 cores, to use those petrographic results to interpret the diagenetic history of Travis Peak sandstones, and to relate the diagenetic history to permeability variations within the formation.
Technical Perspective	Previous work on the Travis Peak has established a regional geologic framework and delineated major depositional systems for the formation across East Texas and North Louisiana. Recent cooperative well activities with operators have yielded several Travis Peak cores, and additional existing core has been loaned or donated to the project. With these cores, it has been possible to begin work on the physical properties of Travis Peak sandstones. This report summarizes the results of petrographic studies of Travis Peak core, including depositional characteristics and diagenetic modifications of the sandstones, and it examines the interplay between diagenesis and permeability.
Results	Travis Peak sandstones are fine to very fine grained quartzarenites and subarkoses that were derived from sedimentary, metamorphic, and igneous rocks exposed in a large area of the southwestern United States. The originally high depositional porosity in matrix-free sandstones has been reduced by compaction and precipitation of authigenic cements, particularly quartz, ankerite, illite, and chlorite. In addition, reservoir bitumen occludes porosity in some zones near the top of the Travis Peak. Primary and secondary porosity and permeability have a wide range of values at the top of the formation, but both the range of values and the maximum values decrease with depth below the top of the Travis Peak. Dissolution of orthoclase and plagioclase has formed most of the secondary porosity. Porosimeter-measured porosity is the best predictor of permeability, and there is a significant inverse correlation between total volume of cement and permeability.

Technical Approach

The petrographic studies utilized 187 thin sections from 10 Travis Peak wells. Petrographic and scanning electron microscopes were used for mineral identification and quantification, and electron microprobe analysis determined feldspar compositions. Relative abundances of clay minerals were determined by X-ray diffraction techniques. Porosity and permeability were measured by routine core analysis and by special techniques designed to simulate in situ conditions. Geochemical studies included elemental analysis of reservoir bitumen.

CONTENTS

Figures

Tables

Plates

INTRODUCTION

Since 1982, the Gas Research Institute (GRI) has supported geological research designed to develop knowledge necessary to effectively exploit low-permeability, gas-bearing sandstones. As part of that program, the Bureau of Economic Geology has been conducting research on the Travis Peak (Hosston) Formation, which is a blanket-geometry, low-permeability sandstone that extends across East Texas, North Louisiana, and southern Mississippi. This effort has been part of a much broader program designed to increase the understanding and ultimate utilization of unconventional gas resources through integration of multiple disciplines involved in tight gas resource development. At present, many tight gas sandstones are not being efficiently evaluated, hydraulically fractured, or produced from because of a lack of appropriate technology to stimulate near-term development of the tight gas resource at competitive prices.

This report presents one aspect of the Bureau's study: determining the composition of Travis Peak sandstones, their diagenetic history, and the causes of their low permeability. Samples of the Travis Peak were available from 10 cores in the East Texas area (fig. 1). Four of these cores are from cooperative wells that were sampled by GRI in conjunction with Travis Peak operators (Clayton W. Williams, Jr. Sam Hughes No. 1, ARCO Oil and Gas Company B. F. Phillips No. 1, Ashland Exploration, Inc. Soil Fertility of Texas [S.F.O.T.] Unit No. 1, and Prairie Producing Company A. T. Mast et al. No. 1-A); the other cores (Amoco Production Company Caldwell Gas Unit No. 2 and M. Kangerga "C" No. 1, Stallworth Oil and Gas, Inc. Everett "B" Oil Unit No. 2 and Renfro Oil Unit No. 2, Sun Oil Company Janie Davis No. 2, and Delta Drilling Company E. Williams "A" No. 1) were contributions from operators.

Petrographic studies of the core have been conducted to determine the grain size and mineral composition of Travis Peak sandstones and mudstones. Diagenetic modifications of the originally deposited sediment were identified using a petrographic microscope, a

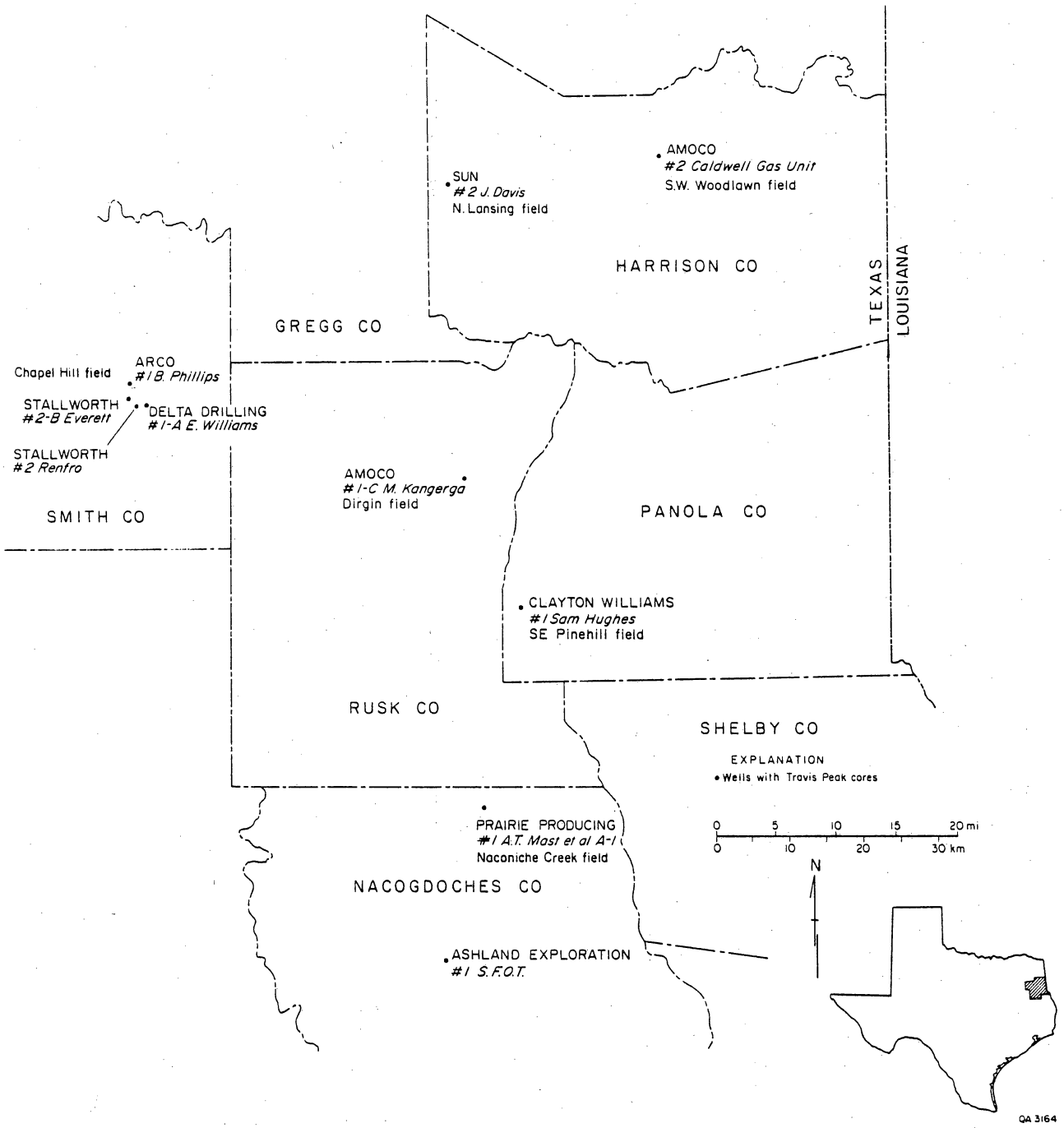

Figure 1. Location of wells from which Travis Peak cores were available.

scanning electron microscope (SEM), and an electron microprobe. Finally, the influence of grain size, detrital mineral composition, and authigenic mineral composition on permeability was evaluated for the Travis Peak Formation in the eastern part of the East Texas Basin.

DEPOSITIONAL HISTORY

The Travis Peak Formation in East Texas was deposited as a complex of high-constructive delta lobes that rapidly prograded over a broad, shallow shelf more than 100 mi wide (Saucier and others, 1985). The Travis Peak deltas prograded onto a relatively competent substrate, so that the delta system spread laterally as well as vertically (fig. 2). As the depocenters shifted back and forth across the stable, shallow shelf, the initial delta deposits were reworked by fluvial processes. Most of the marine sediment was reworked, leaving a sand-rich accumulation of delta-plain and alluvial deposits that is more than 2,000 ft thick in East Texas (fig. 2).

A delta-fringe system formed around the margins of the fluvial-deltaic clastic wedge, and farther offshore, restricted-marine-shelf, shelf-margin, and open-marine systems developed (Saucier and others, 1985). The delta-fringe system includes a variety of depositional environments (or "facies") associated with the transition from the continental fluvial-deltaic system to the shallow-marine-shelf system. The delta fringe contains lithofacies deposited in lower-delta-plain, marsh, lagoon, estuary or bay, tidal-flat, and distributary-bar environments (Finley, 1985). Although the fluvial-deltaic system is the most sand-rich system in the Travis Peak, most of the hydrocarbon production is from the delta-fringe system (Saucier and others, 1985).

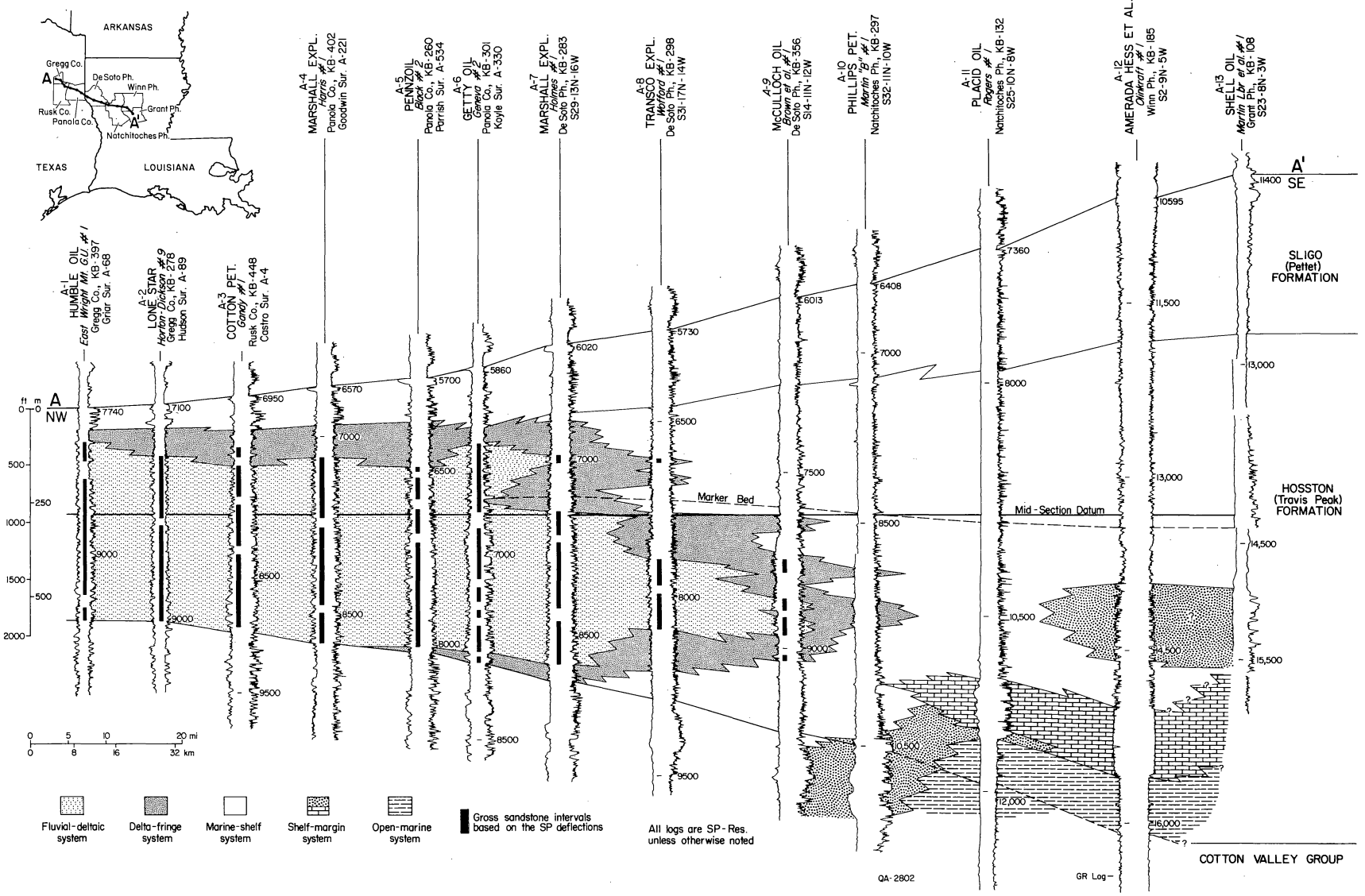

Figure 2. Paleo-dip-oriented stratigraphic cross section A-A', which extends from Gregg County, Texas, to Grant Parish, Louisiana (from Saucier, 1985).

GRAIN SIZE

The Travis Peak Formation in East Texas is composed mainly of sandstones, muddy sandstones, and sandy mudstones (fig. 3). In the four GRI cooperative wells, analysis of framework grain size was accomplished by making grain-size point counts of thin sections. Fifty detrital grains per slide were measured along their long dimension, excluding cement overgrowths. Mean diameter of sand- and silt-size grains was calculated for each sample (tables 1 through 4); detrital and authigenic clays were not included in the calculation of mean grain diameter.

Sandstones

Most of the individual samples have average grain sizes in the fine (.125 to .250 mm) to very fine (.62 to .125 mm) sandstone range (tables 1 through 4). The samples from the Clayton Williams Sam Hughes No. 1 and Ashland S.F.O.T. No. 1 wells had overall average grain sizes of .109 and .117 mm, respectively. The samples from the ARCO Phillips No. 1 and Prairie Mast No. 1-A wells were somewhat coarser, averaging .136 and .138 mm overall.

Samples from existing core contributed by operators were not point counted for grain size, but mean grain size was estimated from thin sections. In general, the estimated grain sizes also averaged in the very fine sandstone to fine sandstone range. Sandstones from the Amoco Kangerga "C" No. 1 well were somewhat coarser than average; several samples were fine sandstones, and the average grain size was .145 mm. Samples from the Sun Janie Davis No. 2 core were relatively fine grained, with an average grain size of .085 mm.

Detrital silt and clay are common in many of the Travis Peak samples. Sandstones with abundant detrital clay were either deposited in a low-energy environment or had clay mixed into an originally clean sandstone by burrowing organisms. In most of the wells there is a significant negative correlation between grain size and matrix content, that is,

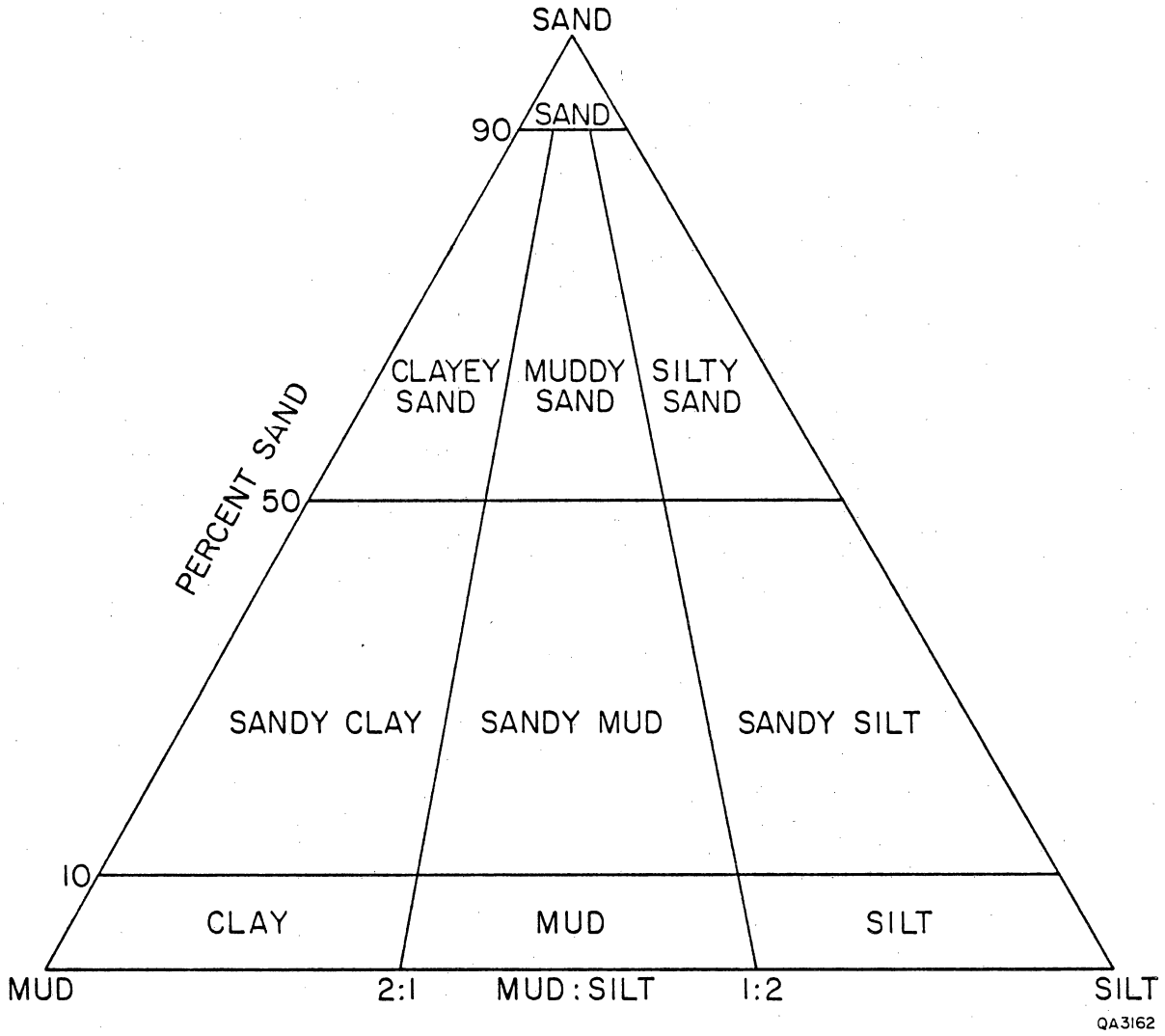

Figure 3. Triangular diagram of terms applied to mixtures of terrigenous sand, silt, and mud (from Folk, 1974).

Table 1. Grain-size distribution in Clayton Williams Sam Hughes No. 1 core.

Depth	Mean (mm)	Sand (%)	Silt (%)	Detrital clay (%)	Authigenic clay (%)	Textural class*
6,835.7	.057	28	58	14	0	Sandy siltstone
6,836.3	.068	48	34	18	0	Sandy mudstone
6,841.5	.075	57	33	10	0	Silty sandstone
6,842.5	.108	90	10	0	0	Sandstone
6,843.7	.104	95	5	0	0	Sandstone
6,851.0	.064	34	42	24	0	Sandy mudstone
7,046.3	.073	54	24	22	0	Muddy sandstone
7,049.4	.078	59	24	17	0	Muddy sandstone
7,061.8	.087	88	10	0	2	Silty sandstone
7,066.1	.087	58	32	10	0	Silty sandstone
7,069.5	.107	76	12	12	0	Muddy sandstone
7,090.3	.100	72	11	17	0	Muddy sandstone
7,093.2	.131	92	2	0	6	Sandstone
7,093.5	.144	92	2	0	6	Sandstone
7,095.3	.127	95	1	0	4	Sandstone
7,097.7	.134	97	0	0	3	Sandstone
7,099.5	.169	98	0	0	2	Sandstone
7,100.2	.143	92	0	0	8	Sandstone
7,101.0	.167	100	0	0	0	Sandstone
7,101.2	.158	96	0	0	4	Sandstone

*Textural class determined only by detrital grains.

Table 2. Grain-size distribution in ARCO Phillips No. 1 core.

Depth	Mean (mm)	Sand (%)	Silt (%)	Detrital clay (%)	Authigenic clay (%)	Textural class*
8,189.6	.120	92	2	0	6	Sandstone
8,190.8	.123	90	0	0	10	Sandstone
8,194.7	.138	70	0	30	0	Clayey sandstone
8,199.6	.118	94	2	0	4	Sandstone
8,211.4	.140	92	2	0	6	Sandstone
8,213.5	.148	94	2	0	4	Sandstone
8,215.0	.204	100	0	0	0	Sandstone
8,216.5	.161	100	0	0	0	Sandstone
8,227.6	.116	90	4	0	6	Sandstone
8,240.6	.114	76	6	6	12	Sandstone
8,243.3	.148	94	0	0	6	Sandstone
8,246.1	.169	92	0	0	8	Sandstone
8,246.8	.184	100	0	0	0	Sandstone
8,257.1	.084	58	28	14	0	Silty sandstone
8,368.8	.126	84	8	8	0	Muddy sandstone
8,372.9	.163	94	4	0	2	Sandstone
8,378.5	.087	70	18	12	0	Muddy sandstone
8,382.0	.116	94	0	0	6	Sandstone
8,385.2	.111	88	4	4	4	Sandstone
8,386.7	.133	100	0	0	0	Sandstone
8,387.5	.144	86	0	14	0	Clayey sandstone

*Textural class determined only by detrital grains.

Table 3. Grain-size distribution in Ashland S.F.O.T. No. 1 core.

Depth (ft)	Mean (mm)	Sand (%)	Silt (%)	Detrital clay (%)	Authigenic clay (%)	Textural class*
9,665.5	.087	70	14	16	0	Muddy sandstone
9,686.3	.055	22	50	28	0	Sandy mudstone
9,697.8	.070	46	42	12	0	Sandy siltstone
9,710.7	.089	74	22	0	4	Silty sandstone
9,715.2	.098	86	12	0	2	Silty sandstone
9,747.1	.130	88	4	6	2	Muddy sandstone
9,750.2	.128	96	4	0	0	Sandstone
9,750.7	.186	100	0	0	0	Sandstone
9,753.0	.130	96	4	0	0	Sandstone
9,753.6	.153	98	2	0	0	Sandstone
9,754.3	.126	96	2	0	2	Sandstone
9,755.6	.127	92	2	0	6	Sandstone
9,757.0	.134	98	0	0	2	Sandstone
9,759.2	.151	98	0	0	2	Sandstone
9,760.3	.123	90	6	0	4	Sandstone
10,085.2	.068	42	36	22	0	Sandy mudstone
10,093.1	.103	80	4	16	0	Clayey sandstone
10,095.9	.100	76	16	8	0	Silty sandstone
10,109.1	.110	90	2	2	6	Sandstone
10,111.0	.164	96	0	0	4	Sandstone
10,112.4	.137	92	4	0	4	Sandstone
10,113.0	.134	94	4	0	2	Sandstone
10,121.0	.094	70	18	12	0	Muddy sandstone
10,127.7	.114	90	2	6	2	Sandstone
10,131.0	.125	100	0	0	0	Sandstone
10,135.0	.131	94	4	0	2	Sandstone
10,141.8	.128	94	4	0	2	Sandstone
10,143.9	.072	50	42	8	0	Sandy siltstone

*Textural class determined only by detrital grains.

Table 4. Grain-size distribution in Prairie Mast No. 1-A core.

Depth (ft)	Mean (mm)	Sand (%)	Silt (%)	Detrital clay (%)	Authigenic clay (%)	Textural class*
8,624	.071	62.0	32.0	2.0	4.0	Silty sandstone
8,624.0	.081	57.8	32.5	9.7	0	Silty sandstone
8,628.0	.063	38.5	45.2	15.3	1.0	Sandy siltstone
8,632.4	.073	49.3	32.8	17.4	0.5	Sandy mudstone
8,639.1	.127	86.0	4.0	0	10.0	Sandstone
8,642.6	.139	89.5	5.7	0	4.8	Sandstone
8,643.9	.114	86.0	9.6	0	4.4	Silty sandstone
8,646.5	.103	92.0	6.0	0	2.0	Sandstone
8,656.3	.090	73.9	20.8	2.4	2.9	Silty sandstone
8,656.9	.080	67.2	26.1	0	6.7	Silty sandstone
8,662.3	.144	90.8	5.8	0	3.4	Sandstone
8,665.0	.077	68.0	29.1	0	2.9	Silty sandstone
8,666.1	.062	35.7	49.4	14.4	0.5	Sandy siltstone
8,667.8	.143	90.7	7.9	0	1.4	Sandstone
8,669.0	.147	93.6	3.9	0	2.5	Sandstone
9,154.9	.193	92.7	1.9	0	5.4	Sandstone
9,161.0	.158	96.6	2.0	0	1.4	Sandstone
9,172.0	.111	76.1	19.0	0	4.9	Silty sandstone
9,186.0	.147	93.7	3.9	0	2.4	Sandstone
9,202.0	.205	98.5	0	0	1.5	Sandstone
9,212.0	.188	98.1	0	0	1.9	Sandstone
9,221.0	.244	98.1	0	0	1.9	Sandstone
9,230.2	.158	93.8	3.9	0	2.3	Sandstone
9,934.9	.104	68.6	26.7	3.3	1.4	Silty sandstone
9,941.1	.114	84.2	11.5	0	4.3	Silty sandstone
9,948.2	.166	98.0	2.0	0	0	Sandstone
9,956.0	.193	96.5	0	0	3.5	Sandstone
9,959.9	.297	99.0	0	0	1.0	Sandstone
9,973.5	.163	82.9	11.3	1.9	3.9	Silty sandstone
9,985.1	.120	90.6	7.9	0	1.5	Sandstone
9,991.1	.126	85.6	5.5	0	8.9	Sandstone

*Textural class determined only by detrital grains.

the fine-grained sandstones tend to have more abundant detrital matrix. The clean sandstones are well sorted and texturally mature, according to the definition of Folk (1974).

Mudstones

True mudstones or claystones (fig. 3) have not been sampled in the Travis Peak cores. Instead, the finest grained layers contain appreciable amounts of silt and sand, so they are texturally classified as sandy mudstones or sandy siltstones (fig. 3). Point counts of four fine-grained samples in the Prairie Mast No. 1-A core illustrate this. All four samples were called mudstones when the cores were described macroscopically. However, thin sections from these intervals revealed that the clay content varied from 30.5 to 79.5 percent, and detrital sand and silt comprised 20 to 69 percent of the detrital volume. Grain-size distributions of these samples are probably typical of the fine-grained beds within the Travis Peak.

TRAVIS PEAK COMPOSITION

A total of 187 thin sections from 10 wells have been point counted to determine mineralogic composition of the Travis Peak (tables 5 through 14); this includes 100 samples from the four GRI cooperative wells (tables 5 through 8). Sandstone composition can be divided into four major parts: (1) framework (i.e., detrital) grains, (2) matrix, (3) porosity, and (4) cement (i.e., authigenic minerals). The relative abundance of each of these four categories has an important influence on permeability.

Framework Grains

Framework grains are divided into essential and nonessential constituents. Essential constituents are those used to classify sandstones: quartz, feldspar, and rock fragments.

Table 5. Petrographic analyses of Clayton Williams Sam Hughes No. 1 core.

	Framework grains										Matrix
Depth (ft)	Quartz	Plagioclase	Orthoclase	MRF*	Chert	Clay clasts	Mica	Heavy minerals	Plant remains	Other	Clay-sized fines
6,835.7	56.0	4.5	0	0	0	0	0	0	0	0	15.0
6,836.3	52.2	2.0	0	0	0.5	0	0	0	0	0	16.4
6,841.5	50.7	6.0	0	0	0	0	0	0	0	0.5	7.0
6,842.5	51.7	2.9	0.5	0	0.5	3.9	0	0	1.0	0	0
6,843.7	50.5	1.9	0	0	0	2.9	0	0.5	0	0	0
6,851.0	66.0	1.5	0	0	0.5	1.0	0	0	0	0	22.2
7,046.3	68.0	3.4	0	0	0	0	0	0	0.5	0	22.7
7,049.4	62.0	1.9	0	0.5	0.5	0	0.5	1.0	0.5	0	25.0
7,061.8	54.0	2.4	0	0	1.4	3.8	0	0	0	0	4.3
7,066.1	65.0	2.0	0	0.5	0.5	0	0	0	0	0	6.4
7,069.5	57.1	2.4	0.9	0	0.5	4.7	0	0	0	0	8.5
7,090.3	66.8	3.9	0	0	0	2.4	0	0	0	0	14.6
7,093.2	61.6	1.5	0	0	0	1.0	0	0	0	0	1.5
7,093.5	58.5	1.4	0	0	1.0	1.4	0	0	0.5	0	0
7,095.3	56.2	2.9	0	0	1.4	0.5	0	0	0.5	0	0
7,097.7	53.6	2.4	0	0.5	0	2.4	0	0	0	0	0
7,099.5	63.2	3.4	0	0	0.5	0	0	0	0	0	0
7,100.2	56.0	2.0	0	1.4	0.5	0.5	0	0	0	0	0
7,101.0	63.8	1.5	0	0	0	0.5	0	0	0.5	0	0
7,101.2	68.5	1.0	0	0	0	0	0	0	0	0	0

*Metamorphic rock fragments

Table 5. (continued)

Depth (ft)	Cements							Porosity	
	Quartz	Dolomite	Ankerite	Authigenic clay	Feldspar	Anhydrite	Solid organic matter	Primary porosity	Secondary porosity
6,835.7	16.0	0	2.0	0	0	0	5.5	0	1.0
6,836.3	19.4	1.0	4.5	0	0.5	0	3.5	0	0
6,841.5	33.8	0	1.0	1.0	0	0	0	0	0
6,842.5	27.8	0	2.9	4.4	0.5	0	0	2.0	2.0
6,843.7	15.6	0	3.8	1.9	0.9	0.5	0	8.7	13.0
6,851.0	4.4	0	3.0	0	0	0	1.5	0	0
7,046.3	3.9	0.5	0	0.5	0.5	0	0	0	0
7,049.4	6.7	1.0	0	0.5	0	0	0	0	0
7,061.8	28.9	0	5.2	0	0	0	0	0	0
7,066.1	16.3	0	7.4	0	0.5	0	1.5	0	0
7,069.5	25.9	0	0.5	0	0	0	0	0	0
7,090.3	11.2	0	0	1.0	0	0	0	0	0
7,093.2	22.7	0	0	2.5	0.5	0	6.9	1.5	0.5
7,093.5	25.6	0	0	4.3	0	0	5.8	1.0	0.5
7,095.3	24.8	0	0	7.1	0	0	0.5	2.4	2.9
7,097.7	22.3	0	0	7.1	0.5	0	0	6.6	4.7
7,099.5	21.1	0	0	2.0	0.5	0	0	5.4	3.9
7,100.2	24.2	0	0	4.8	0	0	1.0	5.3	4.3
7,101.0	27.1	0	0.5	2.4	1.0	1.0	0	1.4	0.5
7,101.2	20.0	0	4.0	3.5	0	0	0	1.0	2.0

Table 6. Petrographic analyses of ARCO Phillips No. 1 core.

	Framework grains										Matrix
Depth (ft)	Quartz	Plagioclase	Orthoclase	MRF*	Chert	Clay clasts	Mica	Heavy minerals	Plant remains	Other	Clay-sized fines
8,189.6	65.2	0.5	0	0.5	0	1.9	0	0	0	0	0
8,190.8	62.7	2.3	0	0	0	1.9	0	0.5	0	0	0
8,194.7	65.7	2.0	0	1.0	0	0	0	0.5	0	0.5	28.9
8,199.6	63.7	1.5	0	0	0	0	0	0	0	0	0
8,211.4	58.7	2.9	0	0	0	8.3	0.5	0	0.5	0.5[1]	0
8,213.5	64.3	2.3	0	1.4	0	0.9	0	0	0	0	0
8,215.0	73.5	3.0	0	0	0	0	0	0	0	1.5[2]	0
8,216.5	72.9	1.5	0	0.5	0	0.5	0	0	0	0.5[1]	0
8,227.6	55.9	2.0	0	0	0.5	0	0	0.5	0	0.5[2]	0
8,240.6	71.1	2.9	0	1.0	0	0.5	0.5	0	0	0	2.5
8,243.3	61.4	2.9	0	0.5	0	2.4	0	0	0	0	0
8,246.1	68.5	3.3	0	0	0	1.4	0	0	0	0	0
8,246.8	67.1	0.5	0	1.0	0	1.0	0.5	0	0	0	0
8,257.1	58.2	0.5	0	0	0	0	0	0	0	0	11.4
8,368.8	71.8	1.9	0	1.4	1.0	0	0	0.5	0	1.0	13.8
8,372.9	70.4	0.5	0	0.5	0	0	0	0	0	0	0
8,378.5	73.3	4.5	0	0	0.5	0	0	0	0	0	5.4
8,382.0	59.0	2.9	0	0.5	0	0.5	0	0.5	0	0	0
8,385.2	67.6	2.8	0.5	0.5	0	5.2	0	0	0	0	5.2
8,386.7	62.4	1.9	0	0	0	2.8	0	0	0	0	0
8,387.5	68.8	0	0	0	1.0	0.5	0	0	0	0.5	10.2

*Metamorphic rock fragments
[1]Pyrite
[2]Fossil fragments

Table 6. (continued)

	Cements								Porosity	
Depth (ft)	Quartz	Dolomite	Ankerite	Fe-calcite	Authigenic clay	Feldspar	Anhydrite	Solid organic matter	Primary porosity	Secondary porosity
8,189.6	24.2	0	0	0	5.3	0	0	2.4	0	0
8,190.8	26.4	0	0.5	0	3.3	0.9	0	1.4	0	0
8,194.7	1.0	0	0	0	0.5	0	0	0	0	0
8,199.6	22.1	1.0	2.5	0	4.4	0	0.5	4.4	0	0
8,211.4	22.8	0	1.9	0	2.9	0.5	0	0	0	0.5
8,213.5	19.7	0	1.9	0	5.6	0.5	0	1.4	0.5	0.9
8,215.0	16.2	0	1.5	3.4	1.0	0	0	0	0	0
8,216.5	13.8	0	1.0	1.0	4.9	0	0	0.5	1.5	1.5
8,227.6	6.9	9.3	10.3	4.9[1]	2.9	0	0	6.4	0	0
8,240.6	13.2	0	1.0	0	5.9	0	0	1.5	0	0
8,243.3	24.2	0	0.5	0	6.3	0	0	0	0.5	1.4
8,246.1	13.9	0	0.5	0	4.2	0	0	0	5.6	2.8
8,246.8	17.4	0	1.0	0	1.0	0	1.0	9.2	0	0.5
8,257.1	12.4	0	0	0	6.5	0	0	10.9	0	0
8,368.8	0.5	0.5	0.5	0	5.3	0	0	0	1.9	0
8,372.9	21.2	0	3.4	1.0	2.5	0	0	0.5	0	0
8,378.5	4.0	0.5	5.0	0	7.4	0	0	0	0	0
8,382.0	22.4	0	0	0	5.4	0	0	6.8	0.5	1.5
8,385.2	13.1	0	0.5	0	4.7	0	0	0	0	0
8,386.7	20.2	0	0.5	0	3.3	0	0	8.9	0	0
8,387.5	14.1	0	0.5	0	1.0	0	0.5[2]	1.5	0	1.5

[1]Calcite
[2]Barite

Table 7. Petrographic analyses of Ashland S.F.O.T. No. 1 core.

	Framework grains										Matrix
Depth (ft)	Quartz	Plagioclase	Orthoclase	MRF*	Chert	Clay clasts	Mica	Heavy minerals	Plant remains	Other	Clay-sized fines
9,665.5	68.8	1.5	0	0	0	0	0	0	0	0.5[1]	11.7
9,666.3	57.1	0.5	1.0	0	0	0	0	0	0	1.5[1]	4.9
9,686.3	55.0	1.5	0	0	0	0	0.5	0	0	0	33.5
9,697.8	64.0	2.0	0	0	0.5	0	0	1.0	0	0	15.3
9,710.7	62.2	3.8	1.4	0.5	0.5	0	0	0.5	4.8	1.0[1]	1.4
9,715.2	58.6	3.9	1.0	1.0	1.0	4.3	0	0	0	1.0[1]	0
9,747.1	76.1	1.5	1.9	0	1.0	0	0	0	0	1.0[1]	10.5
9,750.2	62.9	4.4	0	0	0.5	1.0	0	0	0	0.5[1]	0
9,750.7	63.4	2.0	0	1.0	0.5	0.5	0	0	0	1.0[1]	0
9,753.0	57.6	3.0	0	0.5	0.5	0	0	0	0	0	0
9,753.6	62.6	4.7	0	1.4	0	0.5	0	0	0	0	0
9,754.3	61.5	3.4	0	1.0	0	0.5	0	0.5	0	1.0[2]	0
9,755.6	62.1	5.7	0	0.5	0	0	0	0	0	0.9[2]	0
9,757.0	60.1	1.5	2.0	0.5	0.5	0.5	0	0.5	0	0	0
9,759.2	65.5	1.5	0	0.5	0	0	0	0	0	0	0
9,760.3	69.6	3.0	0	1.0	0	1.0	0	0	0	0.5[3]	0
10,085.2	63.2	1.0	1.0	0	0.5	2.0	0	0	0	0	17.9
10,093.1	69.3	2.0	0	0	0.5	1.5	0	0	0	0.5[3]	11.9
10,095.9	70.2	2.9	1.4	0.5	0	1.0	0	0.5	0	0	9.1
10,109.1	61.5	3.4	1.9	0	0	3.4	0	0	0	0	2.9
10,111.0	65.9	3.8	0.5	0.5	0	0	0	0	0	0	0
10,112.4	62.1	2.0	0	0	0	0	0	0	0	0	0
10,113.0	67.0	4.3	1.0	0.5	0.5	0.5	0	0	0	0.5[2]	1.0
10,121.0	72.8	1.5	1.0	0.5	0	0	0	0.5	0	0.5[4]	13.1
10,127.7	64.5	2.5	1.0	1.0	0.5	0	0	0	0	0.5[4]	6.4
10,131.0	70.2	1.5	1.0	0.5	0.5	1.5	0	0	0.5	0.5[3]	0
10,135.0	70.4	2.5	0	0	0.5	0.5	0	0	0	0	0
10,141.8	67.6	1.0	1.5	3.4	1.0	1.0	0	0	0	0.5[3]	0
10,143.9	66.3	0	1.5	1.0	0	0.5	0	0	0	0	14.1

*Metamorphic rock fragments
[1]Pyrite
[2]Grains altered to clay
[3]Hematite
[4]Opaque

Table 7. (continued)

	Cements								Porosity	
Depth (ft)	Quartz	Dolomite	Ankerite	Authigenic clay	Feldspar	Anhydrite	Solid organic matter	Fe-calcite	Primary	Secondary
9,665.5	2.9	2.9	1.0	0.5	0	0	5.4	0	0	4.9
9,666.3	0	16.1	19.0	0	0	0	0	0	0	0
9,686.3	0	7.0	2.5	0	0	0	0	0	0	0
9,697.8	13.3	1.0	1.0	2.0	0	0	0	0	0	0
9,710.7	13.4	1.9	2.9	5.3	0.5	0	0	0	0	0
9,715.2	21.9	0	3.8	3.8	0	0	0	0	0	0
9,747.1	5.7	1.0	0.5	1.0	0	0	0	0	0	0
9,750.2	21.0	2.4	4.4	2.4	0.5	0	0	0	0	0
9,750.7	21.0	0.5	1.0	2.0	0	0	2.9	0	0	4.4
9,753.0	18.7	8.9	6.9	1.0	0	0	0	0	0	3.0
9,753.6	17.5	2.4	7.1	1.8	0	0	0	0	0	1.9
9,754.3	11.7	7.8	5.9	2.4	0	0	0	0	0	4.4
9,755.6	10.4	3.3	5.2	6.2	0	0	0	0	0	5.7
9,757.0	16.3	1.4	1.4	8.7	0	0	0	0	0	6.7
9,759.2	22.7	0.5	2.0	3.4	0	0	0	0	1.5	2.5
9,760.3	16.2	2.0	2.5	2.9	0	0	0	0	0	1.5
10,085.2	6.5	1.0	6.5	0	0	0	0.5	0	0	0
10,093.1	8.9	0	1.5	3.0	0	0	0	0	0.5	0.5
10,095.9	8.7	0	0.5	2.9	0	0	0	0	0	2.4
10,109.1	8.2	3.8	5.8	5.8	0	0	0	0	0	3.4
10,111.0	16.8	1.0	1.0	3.8	0	0	0.5	0	0.5	5.8
10,112.4	20.7	1.0	1.5	2.0	0	0	0	0	2.0	8.4
10,113.0	10.5	1.0	1.4	5.7	0	0	0	0	0.5	5.7
10,121.0	1.9	3.9	3.4	0	0	0	1.0	0	0	0
10,127.7	10.8	0	0.5	6.4	0.5	0	0	0	2.5	3.0
10,131.0	22.4	0	0.5	0.5	0	0	0	0	0.5	0
10,135.0	16.7	0	1.0	4.9	0	0.5	0	0	1.0	2.0
10,141.8	23.0	0	0	1.0	0	0	0	0	0	0
10,143.9	0.5	2.4	13.7	0	0	0	0	0	0	0

Table 8. Petrographic analyses of Prairie Mast No. 1-A core.

	Framework grains										Matrix
Depth (ft)	Quartz	Plagioclase	Orthoclase	MRF*	Chert	Clay clasts	Mica	Heavy minerals	Pyrite	Other	Clay-sized fines
8,624.0	61.7	3.9	0.5	0	0	0	0	0	0	0	9.7
8,628.0	70.3	4.0	0.5	0	0	0	0	0	0	0	15.3
8,632.4	65.2	2.9	1.4	0.5	0	0	0	0	0	0	17.4
8,639.1	64.9	1.0	0	0.5	1.0	1.0	0	0.5	0	0	0
8,642.6	68.6	2.9	1.4	0	0	0	0	0	0	0	0
8,643.9	59.7	2.9	0.5	0.5	0.5	0	0.5	0	0	0	0
8,646.5	64.5	3.0	0	1.0	0	1.0	0	0	0	0	0
8,656.3	63.3	5.2	1.0	1.0	0.5	0	0	0	0	0	2.4
8,656.9	59.6	4.3	2.4	0.5	0.5	1.0	0.5	0	0.5	0	0
8,662.3	68.4	1.5	1.9	0	0.5	0	0	0	0	0	0
8,665.0	57.6	4.4	2.0	0.5	0	3.4	0	0	0	0	0
8,666.1	52.9	7.7	1.9	1.0	1.0	4.8	0	0	1.4	0.5[2]	14.4
8,667.8	57.4	2.9	1.9	0.5	1.0	1.0	0	0	0	0.5[1]	0
8,669.0	60.6	3.4	0.5	0	0	0	0	0	0	0	0
9,154.9	68.8	3.4	0.5	0	0	0.5	0.5	0.5	0	0	0
9,161.0	63.3	1.0	1.9	1.0	1.0	0.5	0.5	0	0	0	0
9,172.0	64.2	4.4	0	0.5	0	0.5	0	1.0	0	0	0
9,186.0	66.0	4.2	2.8	0	0.9	0	0	0	0	0	0
9,202.0	66.2	2.5	0.5	0	0.5	0	0	0	0	0	0
9,212.0	62.6	2.9	1.0	0	0.5	0.5	0	0	0	0	0
9,221.0	68.7	1.9	0.5	0.9	0.5	3.8	0	0	0.9	0.5	0
9,230.2	70.0	6.0	3.7	0	0	0	0	0	0	0	0
9,934.9	63.4	2.8	0	0	0	4.2	0.5	0.5	0.9	3.8[1]	3.3
9,941.1	64.9	2.4	0	0	0	0	0	0	0	1.9[1]	0
9,948.2	71.6	2.5	0	0.5	0.5	0	0	0	0	0	0
9,956.0	70.0	0	0	0	1.5	0	0	0	0	0	0
9,959.9	76.4	1.0	0	0.5	0	0	0	0	0	0	0
9,973.5	68.4	2.4	0	0.5	0.5	1.9	0	0	0.5	1.5[1]	1.9
9,985.1	68.3	1.5	0	0	0.5	0	0	0.5	0.5	0	0
9,991.1	63.5	1.5	0	0	0.5	0	0	0	7.9	0	0

*Metamorphic rock fragments
[1]Grain altered to clay
[2]Coalified wood

Table 8. (continued)

	Cements							Porosity	
Depth (ft)	Quartz	Dolomite	Ankerite	Authigenic clay	Feldspar	Anhydrite	Solid organic matter	Primary	Secondary
8,624.0	5.8	8.7	8.7	0	0	0	0	0	1.0
8,628.0	2.0	3.5	1.0	1.0	0	0	0	0	2.5
8,632.4	2.4	3.4	2.9	0.5	0	0	2.4	0.5	0.5
8,639.1	18.5	0	2.0	10.2	0	0	0	0	0
8,642.6	20.8	0	0.5	4.8	0	0.5	0	0.5	0
8,643.9	22.8	0.5	1.5	4.4	0.5	0	0	2.4	3.4
8,646.5	16.7	0	5.9	2.0	0	0	0	1.0	4.9
8,656.3	11.4	1.0	7.6	2.9	0	1.0	0	1.9	1.0
8,656.9	18.3	0	4.8	6.7	0	0	0	0.5	0.5
8,662.3	15.5	0	7.3	3.4	0	0.5	0	0	1.0
8,665.0	18.5	1.5	9.3	2.9	0	0	0	0	0
8,666.1	4.8	2.4	6.7	0.5	0	0	0	0	0
8,667.8	23.9	0	7.2	1.4	0	0	0	1.0	1.4
8,669.0	19.7	0	10.8	2.5	0	0	0	1.5	1.0
9,154.9	11.2	1.5	5.4	5.4	0	0.5	0	1.0	1.0
9,161.0	19.0	0	4.3	1.4	0.5	0	0	1.9	3.8
9,172.0	15.7	2.5	6.4	4.9	0	0	0	0	0
9,186.0	19.3	0	0	2.4	0	0	0	0.9	3.3
9,202.0	23.5	0	0.5	1.5	0	0	0	1.0	3.9
9,212.0	14.1	0.5	2.9	1.9	0	8.7	0	0.5	3.9
9,221.0	13.7	0	0	1.9	0	0	0	0.9	5.2
9,230.2	15.2	0.5	0.5	2.3	0.5	0	0	0	1.4
9,934.9	16.9	0	0.5	1.4	0.5	0	0	0	1.4
9,941.1	23.1	0	0	4.3	0.5	0	0	0	2.4
9,948.2	21.6	0	0	0	0	0	0	1.0	2.5
9,956.0	21.0	0	0	3.5	0	0	0	1.0	3.0
9,959.9	18.2	0	0	1.0	0	0	0	1.0	2.0
9,973.5	18.0	0	0	3.9	0	0	0	0	0.5
9,985.1	22.8	0	0	1.5	0	0	0	0.5	4.0
9,991.1	14.8	0	0	8.9	0	0	0	0	3.0

Table 9. Petrographic analyses of Amoco Caldwell Gas Unit No. 2 core.

Depth (ft)	Framework grains										Matrix
	Quartz	Plagioclase	Orthoclase	MRF*	Chert	Clay clasts	Mica	Heavy minerals	Pyrite	Other	Clay-sized fines
6,816.6	74.4	2.0	0	1.0	0	0	0	0.5	0	0.5[1]	0
6,825.2	77.3	1.0	0	0	0.5	0	0	0	0	0	0
6,831.5	69.4	5.3	0	1.0	0	0	0	0	0	0	0
6,837.6	67.8	3.5	0	1.0	0	0	0	0	0	0	0
6,848.4	67.2	1.0	0	0.5	1.0	2.5	0	0	0	0	7.0
6,889.5	75.2	2.0	0	0.5	0	0.5	0	0	0	0	0
6,899.3	65.2	2.0	0	2.5	0	2.0	0	0	0	0	12.9
6,907.6	67.2	1.0	0	1.0	1.0	13.7	0	0	0	1.0[1]	2.0
7,240.0	70.0	2.0	0	0.5	1.0	1.0	0	0	0	0	0
7,255.5	67.5	4.3	0.5	0.5	1.4	0	0	0	0	0	0
7,260.3	64.0	3.4	0	0	1.0	0	0	0	0	0	0
7,263.3	64.7	3.4	0	0	0	0.5	0	0	0	0	0
7,276.4	68.4	2.9	0	1.0	1.5	0.5	0	0	0	0	0
7,295.5	65.0	3.5	0	1.0	0	0	0	0	0	0	0
7,315.9	68.7	2.0	0	0	1.0	0	0	0	0	0	0
7,317.4	68.3	1.5	0	0	0	0.5	0	0	0	0	0
7,325.2	68.0	3.4	0	0.5	1.5	1.0	0	0	0	0	0
7,339.7	64.9	3.8	0	0.5	0	0.5	0	0	0	1.0[1]	0
7,341.0	66.7	4.8	0	0	1.0	0.5	0	0	0	0	0
7,349.6	69.7	2.9	0	0	0	1.9	0	0	0	0	3.4
7,354.3	70.9	1.5	0	1.9	0	0.5	0	0	0	0	0
7,358.3	68.3	3.8	0.5	0.5	0.5	1.9	0	0	0	0	1.4

*Metamorphic rock fragments
[1]Grain altered to clay

Table 9. (continued)

Depth (ft)	Cements							Porosity	
	Quartz	Dolomite	Ankerite	Authigenic clay	Feldspar	Anhydrite	Solid organic matter	Primary	Secondary
6,816.6	16.7	0	1.0	1.5	0.5	0	0	1.0	1.0
6,825.2	14.8	0	1.5	3.0	0	0	0	2.0	0
6,831.5	18.9	0	1.9	1.0	0.5	0	0	1.5	0.5
6,837.6	24.3	0	0.5	2.0	0	0	0	1.0	0
6,848.4	17.9	0	0	2.5	0.5	0	0	0	0
6,889.5	17.3	0	2.0	2.5	0	0	0	0	0
6,899.3	14.4	0	0	0	0	0	0	0	1.0
6,907.6	11.3	0	0	1.5	0	0	0	0	0.5
7,240.0	18.7	1.0[2]	3.9	0	0	0	0	1.0	1.0
7,255.5	14.8	0.5	1.9	1.0	0.5	0	0	1.4	5.7
7,260.3	22.7	0	1.0	1.5	0	0.5	0	0.5	5.4
7,263.3	16.2	1.5	1.5	2.5	0	0	0	0	9.8
7,276.4	13.1	3.9	2.9	0.5	0	0	0	0	5.3
7,295.5	17.5	0.5	1.0	3.0	0	1.5	0	0	7.0
7,315.9	16.4	0	1.0	0.5	0.5	0	3.5	0.5	6.0
7,317.4	18.3	1.5	2.5	1.0	0	0	0	2.5	4.0
7,325.2	12.1	0	1.0	6.3	0	0	0	2.4	3.9
7,339.7	11.1	1.4	1.9	7.2	0.5	0	0	1.9	5.3
7,341.0	14.0	0.5	2.4	1.0	0	1.4	0	0.5	7.2
7,349.6	11.5	1.9	3.4	0.5	0	0	0	1.0	3.8
7,354.3	15.0	0.5	0.5	1.5	0	0	0	2.4	5.3
7,358.3	10.1	2.9	1.4	6.3	0.5	0.5[3]	0	1.0	0.5

[2]Calcite nodule
[3]Barite cement

Table 10. Petrographic analyses of Amoco Kangerga "C" No. 1 core.

Depth (ft)	Framework grains										Matrix
	Quartz	Plagioclase	Orthoclase	MRF*	Chert	Clay clasts	Mica	Heavy minerals	Pyrite	Other	Clay-sized fines
8,409.8	64.1	3.8	0	0	0	0.5	0	0	0	0.5[1]	0
8,417.3	71.1	1.0	0	0.5	0	0	0	0	0	0	0
8,419.0	74.4	1.4	0	1.0	0	0.5	0	0	0	0	0
8,420.9	65.9	3.3	0	1.9	0	0.9	0	0	0	0.5[2]	0
8,466.5	67.9	4.2	0	2.3	0	0	0.5	0	0	0	0
8,470.3	71.8	3.4	0	0.5	1.0	0	0	0	0	0.5[3]	0
8,478.5	68.4	1.9	0	0.5	2.4	0	0	0.5	0	0	0
8,504.5	68.0	2.9	0	2.4	0.5	0.5	0	0	0	0	0
8,518.1	64.0	2.0	0	2.5	1.5	1.0	0.5	0	0	0	16.5
8,541.0	65.0	5.8	0	0.5	1.0	0.5	0	0	0	0	0
8,574.4	58.6	3.4	0	1.5	0.5	0.5	0	0	0	0	25.1
8,596.0	66.3	0.5	0	1.0	0	0	0	0	0	0	0
8,599.0	77.1	1.5	0	1.0	1.0	0	0	0	0	0	0
8,602.0	73.1	1.9	0	0.5	1.9	0.5	0	0	0	0.5[3]	0
8,604.1	68.6	1.0	0	1.0	0.5	0	0	0	0	0.5[2]	0
8,618.4	68.1	2.9	0	1.9	1.0	0	0	0.5	0	0	0
8,627.2	75.4	1.4	0	1.9	1.4	0	0	0	0	0	0.5
8,633.8	67.7	1.5	0	1.0	0.5	0	0	0	0	0.5[4]	0
8,637.9	69.4	1.4	0	2.3	3.2	1.4	0	0	0.5	0	0
8,638.5	69.4	3.3	0	1.9	1.4	3.3	0	0	0	0	0
8,644.6	68.7	3.3	0	1.4	0.9	0.9	0.5	0	0	0	0
8,650.0	68.6	2.4	0	1.0	1.4	0.5	0	0.5	0	0	0
8,656.6	70.1	0.5	0	0.5	2.0	0	0	0	0	0	10.0
8,660.2	71.3	3.0	0	1.0	0	0	0	0.5	0	0	3.5
8,662.6	71.6	1.0	0	2.0	1.5	0.5	0	0	0	0	0

*Metamorphic rock fragments
[1]Hematite
[2]Plutonic rock fragment
[3]Barite cement
[4]Volcanic rock fragment

Table 10. (continued)

Depth (ft)	Cements								Porosity	
	Quartz	Dolomite	Ankerite	Fe-calcite	Authigenic clay	Feldspar	Anhydrite	Solid organic matter	Primary	Secondary
8,409.8	29.2	0	0	0	1.0	0	0	0	0	1.0
8,417.3	11.4	0	10.4	0	0	0	2.0	0	0	3.5
8,419.0	15.9	0	0	0	0	0.5	2.9	0	0.5	2.9
8,420.9	19.4	0	0.5	0	1.4	0	2.4	0	0.5	3.3
8,466.5	17.2	0.5	0	0	1.9	0.9	0	0	0.9	3.7
8,470.3	18.0	0	0	0	0	0	1.0	0	0	4.4
8,478.5	18.4	0	0.9	0	1.4	0	0	0	0.9	4.7
8,504.5	16.0	0	0	0	4.9	0	0	0	1.5	3.4
8,518.1	6.5	0	0	0	0.5	0	0	0	1.5	3.5
8,541.0	20.4	0	1.0	0	0.5	0	0	0	1.0	4.4
8,574.4	10.3	0	0	0	0	0	0	0	0	0
8,596.0	24.8	0	0	0	0.5	0	0	0	0.5	6.4
8,599.0	14.1	0	0	0	1.5	0	0	0	1.0	2.9
8,602.0	16.8	0	0	0	1.4	0	0	0	1.4	1.9
8,604.1	15.2	0	0.5	0	4.4	0	0	0	2.5	5.9
8,618.4	12.6	0	1.4	0	4.8	0	0	0	1.9	4.8
8,627.2	9.2	0	0	0	7.7	0	0	0	0	2.4
8,633.8	27.9	0	0	0	1.0	0	0	0	0	0
8,637.9	20.4	0	0.5	0	0.9	0	0	0	0	0
8,638.5	17.2	0	0	0	2.9	0.5	0	0	0	0
8,644.6	20.4	0	0	0	3.3	0	0	0	0	0.5
8,650.0	22.7	0	0	0	1.9	0	0	0	0	1.0
8,656.6	16.4	0	0	0	0.5	0	0	0	0	0
8,660.2	20.8	0	0	0	0	0	0	0	0	0
8,662.6	20.9	0	0	0	1.0	0	1.0	0	0.5	0

Table 11. Petrographic analyses of Sun Janie Davis No. 2 core.

	Framework grains										Matrix
Depth (ft)	Quartz	Plagioclase	Orthoclase	MRF*	Chert	Clay clasts	Mica	Heavy minerals	Pyrite	Other	Clay-sized fines
7,496.9	65.4	3.4	0	0	0	1.0	0	0	0	0	0.5
7,497.1	61.8	3.9	0	0	0	0.5	0	0	0	0.5[1]	0
7,542.4	68.4	1.5	0	0	0	0.5	0	0.5	0	0.5[1]	0
7,552.6	73.3	0.5	0	0.5	0	0	0.5	0	0	0	6.4
7,575.1	61.1	1.5	0	0	0	0.5	0	0	0	0.5[1]	0
7,584.4	63.4	5.0	0	0.5	0	0	0	0	0	0	0
7,590.0	58.5	3.9	0	0	0	0.5	0	0	0	1.4[1]	0
7,603.6	64.4	2.4	0	0	0	1.4	0	0	0	2.4[1]	0

*Metamorphic rock fragments
[1]Grain altered to clay

	Cements							Porosity	
Depth (ft)	Quartz	Dolomite	Ankerite	Authigenic clay	Feldspar	Anhydrite	Solid organic matter	Primary	Secondary
7,496.9	10.7	1.5	3.4	6.8	0	0	0	1.0	6.3
7,497.1	11.8	1.5	3.9	3.9	0	0	6.4	2.0	3.9
7,542.4	13.1	0.5	0	5.8	0.5	0	5.3	1.0	2.4
7,552.6	3.5	0	0.5	3.0	0	0	11.9	0	0
7,575.1	15.3	0	0	1.5	0.5	0	6.9	2.0	10.8
7,584.4	12.9	2.5	4.5	6.9	0	0	0	0.5	4.0
7,590.0	11.6	1.0	10.1	5.8	0	0	0	1.0	6.3
7,603.6	23.6	0	0	3.8	0	0	0	1.0	1.0

Table 12. Petrographic analyses of Stallworth Everett "B" No. 2 core.

Depth (ft)	Framework grains										Matrix
	Quartz	Plagioclase	Orthoclase	MRF*	Chert	Clay clasts	Mica	Heavy minerals	Pyrite	Other	Clay-sized fines
8,155.7	58.8	4.9	0	0	1.0	1.0	0	0	0.5	0	7.4
8,175.7	63.5	2.5	0	0	1.0	4.9	0	0	0	1.5[1]	1.0
8,178.7	59.2	1.0	0	0	1.0	2.5	0	0	0.5	0	0
8,179.1	61.7	1.5	0	0	0	6.0	0	0	0	0	0.5
8,186.5	68.8	3.0	0	0.5	0	0	0.5	0	0	0	7.4
8,191.2	67.7	1.5	0	0	0	0.5	0	0	0	0.5[2]	29.9
8,227.8	68.5	2.0	0.5	0	0	0	0	0.5	0	0	0
8,230.5	70.0	1.0	1.0	0	0.5	0	0.5	0	0	0.5[1]	0
8,231.5	65.0	2.5	0	1.0	0	1.0	0	0	0	0	0
8,240.0	67.5	1.0	0	0.5	0	0.5	0	0	0	1.0[1]	0
8,261.1	66.3	0	0.5	0	0	1.0	0	0	2.0	3.4[2]	0
8,265.5	68.2	0	0	0.5	0	5.5	0	0	0.5	0.5[2]	3.5
8,316.9	74.6	1.5	0	0	0.5	0	0	0	0	0	10.9
8,328.0	80.1	2.0	0	0	0	0	0	0	0	0	11.4
8,349.6	69.3	3.9	0	0.5	0	0	0	0.5	0	0	14.1
8,355.9	80.0	2.0	0	0	0	0	0	0	0	0	4.0
8,366.9	69.7	2.0	0	0	0	1.0	0	0.5	0	0	0

*Metamorphic rock fragments
[1]Grain altered to clay
[2]Coalified wood

Table 12. (continued)

Depth (ft)	Cements							Porosity	
	Quartz	Dolomite	Ankerite	Authigenic clay	Feldspar	Anhydrite	Solid organic matter	Primary	Secondary
8,155.7	20.1	1.5	4.4	0	0	0	0	0	0.5
8,175.7	21.2	1.0	0.5	2.0	0	0	1.0	0	0
8,178.7	16.4	0.5	0	0.5	0	0	18.4	0	0
8,179.1	11.4	3.5	0.5	0	0.5	0	14.4	0	0
8,186.5	18.3	0	0.5	0	0	0	1.0	0	0
8,191.2	0	0	0	0	0	0	0	0	0
8,227.8	19.7	0.5	0	8.4	0	0	0	0	0
8,230.5	9.9	0.5	1.0	3.4	0	0	11.8	0	0
8,231.5	15.3	1.0	2.0	3.9	0.5	0	7.9	0	0
8,240.0	15.3	0	1.0	8.9	0	0	4.4	0	0
8,261.1	13.2	2.9	5.9	4.9	0	0	0	0	0
8,265.5	16.4	0	1.0	3.5	0	0	0.5	0	0
8,316.9	10.4	0	0	0	0	0	2.0	0	0
8,328.0	6.5	0	0	0	0	0	0	0	0
8,349.6	7.8	0.5	2.0	0	0	0	0.5	0	1.0
8,355.9	5.0	1.0	3.0	5.0	0	0	0	0	0
8,366.9	15.4	1.0	0.5	5.0	0	0	2.0	0	3.0

Table 13. Petrographic analyses of Stallworth Renfro No. 2 core.

	Framework grains										Matrix
Depth (ft)	Quartz	Plagioclase	Orthoclase	MRF*	Chert	Clay clasts	Mica	Heavy minerals	Pyrite	Other	Clay-sized fines
8,181.2	62.9	2.0	0	0	0	3.9	0	0.5	0	0	0
8,189.9	72.8	4.5	0	0	0	0	0	0	0	0	14.4
8,225.5	66.5	2.9	0	1.0	0	0	0.5	0	0	0	9.7
8,229.0	69.3	3.9	0	1.0	0.5	0	0	0.5	0	0	11.7
8,230.8	64.0	1.5	0	0.5	1.0	4.9	0	0	0	0	11.8
8,232.7	56.4	2.0	0	0	0	1.5	0	0	0	0	0

*Metamorphic rock fragments

	Cements							Porosity	
Depth (ft)	Quartz	Dolomite	Ankerite	Authigenic clay	Feldspar	Anhydrite	Solid organic matter	Primary	Secondary
8,181.2	13.2	0	0	1.5	0.5	0	15.6	0	0
8,189.9	0.5	6.4	1.5	0	0	0	0	0	0
8,225.5	18.4	0	0	0	1.0	0	0	0	0
8,229.0	10.7	0	0	0	0	0	2.4	0	0
8,230.8	13.3	0	0.5	0	0	0	0.5	1.5	0.5
8,232.7	16.8	0	3.0	1.0	0	0	19.3	0	0

Table 14. Petrographic analyses of Delta Williams "A" No. 1 core.

	Framework grains										Matrix
Depth (ft)	Quartz	Plagioclase	Orthoclase	MRF*	Chert	Clay clasts	Mica	Heavy minerals	Pyrite	Other	Clay-sized fines
8,171.0	61.5	2.0	0	0.5	0	0	0	0	0	0	4.0
8,185.5	61.6	4.3	0	0.9	0	3.3	0	0	0	0	0
8,188.3	61.0	0.5	0	2.0	1.0	0	0	0	0	0	0
8,188.5	65.2	1.5	0	0.5	0	1.5	0	0	0	0	8.8
8,190.1	44.3	1.5	0	0.5	0.5	0	0	0	0	0	1.5
8,193.8	58.7	1.0	0	0.5	1.0	0	0	0	0	0.5[1]	0
8,199.6	67.0	2.0	0	0.5	0	3.5	0	0	0	0	4.5
8,204.3	62.7	1.5	0	0.5	0	1.0	0	0.5	0	0	9.5
8,215.1	61.5	1.5	0	1.0	0.5	2.0	0	0	0	0	5.5

*Metamorphic rock fragments
[1]Grain altered to clay

	Cements							Porosity	
Depth (ft)	Quartz	Dolomite	Ankerite	Authigenic clay	Feldspar	Anhydrite	Solid organic matter	Primary	Secondary
8,171.0	2.5	8.0	19.5	0	0	0	2.0	0	0
8,185.5	16.1	0	1.9	0.9	0	0	0.5	1.9	8.5
8,188.3	16.5	0	1.5	1.5	0	0	16.0	0	0
8,188.5	14.7	0	1.0	2.0	0.5	0	0	0.5	3.9
8,190.1	1.0	34.3	16.4	0	0	0	0	0	0
8,193.8	17.9	0	1.5	0.5	0	0	18.4	0	0
8,199.6	16.5	1.0	2.0	2.5	0	0	0	0.5	0
8,204.3	19.9	0	0.5	1.5	0	0	2.0	0	0.5
8,215.1	19.0	0	2.5	2.5	0	0	4.0	0	0

Any other detrital grains, including redeposited rip-up clay clasts, are nonessential to sandstone classification.

Essential Constituents

Quartz is the most abundant detrital mineral in all Travis Peak samples (pl. IA). It comprises up to 80 percent of the sandstone volume and averages 65.4 percent. Of the essential constituents, detrital quartz constitutes 82 to 99 percent. Most detrital quartz grains are single crystals with straight or slightly undulose extinction, although polycrystalline quartz grains are present.

Detrital feldspar (including plagioclase, orthoclase, and microcline) forms 0 to 10 percent of the total rock volume (tables 5 through 14), and 0 to 15 percent of the essential constituents. Plagioclase is more abundant than orthoclase in all wells, and microcline is extremely rare. The average volume of feldspar in the four GRI cooperative wells is 2 to 3 percent (tables 5 through 8); the Ashland S.F.O.T. No. 1 and Prairie Mast No. 1-A cores average 3.5 percent, whereas the Clayton Williams Sam Hughes No. 1 and ARCO Phillips No. 1 cores contain significantly less feldspar (an average of 2.3 percent). Much of the plagioclase is untwinned, indicating it had a metamorphic origin (Folk, 1974). Plagioclase grains vary from fresh to sericitized and vacuolized. Partial dissolution of plagioclase along cleavage planes results in delicate skeletal grains and secondary porosity (pl. IB). Many grains have albite twinning, but other grains have a patchy, indistinct type of twinning called "chessboard" that may be caused by albitization and healing of partially dissolved plagioclase (Gold, 1984). Plagioclase grains in the Travis Peak samples have been extensively albitized (see Feldspar section, p. 42).

Orthoclase and microcline are rare in all cores (average = .05 percent in Clayton Williams Sam Hughes No. 1 and ARCO Phillips No. 1), except in the Ashland S.F.O.T. No. 1 and Prairie Mast No. 1-A cores, where they average 0.8 percent of the rock volume. The significantly greater volume of total feldspar in the Ashland S.F.O.T. No. 1 and Prairie

Mast No. 1-A samples is accounted for by the greater volume of orthoclase; there is no significant difference in plagioclase content in the Ashland and Prairie cores compared to the Clayton Williams and ARCO cores. The presence of more potassium feldspar in the Ashland S.F.O.T. No. 1 and Prairie Mast No. 1-A cores suggests that orthoclase may originally have been more abundant in the other cores as well, but was removed by dissolution during burial. It is not known why significantly more orthoclase remains in those two wells; perhaps their greater depth below the top of the Travis Peak or their more downdip location in comparison to the other cores is part of the explanation. Alternatively, more orthoclase may originally have been deposited in the area of these two wells. Possible differences in source areas tapped by different fluvial axes may have resulted in local variations in sandstone composition in different local depocenters.

Rock fragments are primarily chert and metamorphic rock fragments in the Travis Peak. Each is generally present in volumes of 0 to 1 percent. Many of the samples also contain a trace of very fine grained siliceous rock fragments. Their origin is not known, but they appear to be either metamorphosed fine siltstone or metamorphosed chert whose grain size increased during metamorphism. The presence of these three types of rock fragments indicates that the source area for the Travis Peak included both sedimentary and metamorphic rocks.

Clay clasts are common (tables 5 through 14), but they were derived locally when partially consolidated mud layers were ripped up and redeposited with sand. Because of their local origin, clay clasts were not included in the rock fragment category when the sandstones were classified.

Provenance

The essential constituents provide information about the provenance of Travis Peak sandstones. These sandstones are quartzarenites and subarkoses (fig. 4), and the average composition (quartz, feldspar, rock fragments) for all the samples is $Q_{94.7}\ F_{4.0}\ R_{1.3}$. The

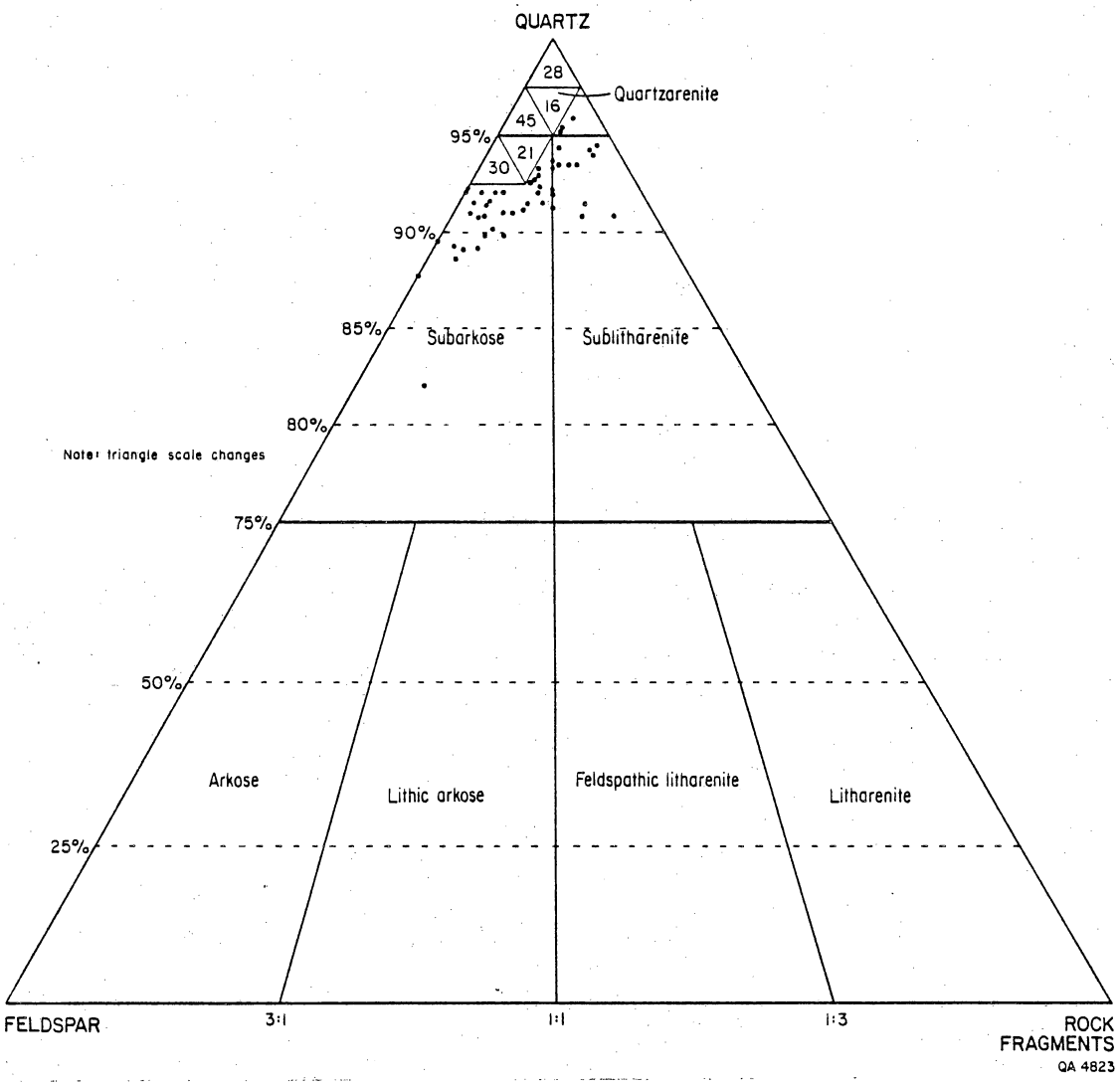

Figure 4. Classification of Travis Peak sandstones (from Folk, 1974).

high percentage of quartz indicates these samples are mineralogically mature; unstable grains either were not abundant in the source area, or they were removed during transportation, deposition, and burial, or both. Work by Saucier (1985) indicates that the Travis Peak was derived from a large area of the southwestern United States that included sedimentary, metamorphic, and igneous rocks. The high percentage of quartz in the Travis Peak is probably caused at least in part by the presence of abundant sedimentary rocks in the source areas. Metamorphic rocks contributed slate and phyllite fragments, metachert, and much of the plagioclase. Granitic Precambrian basement exposed in Oklahoma and Colorado during the Early Cretaceous also contributed feldspar and quartz, as well as plutonic rock fragments. However, plutonic rock fragments are rare in the Travis Peak sandstones because igneous rocks were a minor part of the source terrain and because the transport distance was sufficiently long that most rock fragments were broken into mineral grains, particularly quartz and feldspar.

Nonessential Constituents

Other framework grains (nonessential constituents) not used to classify the sandstones are present in the Travis Peak in varying amounts. Tourmaline and zircon, which are both extremely stable, are the only heavy minerals observed in thin section. They can survive long transport distances and can be recycled from older sedimentary rocks. The lack of other heavy minerals may be attributed to two factors. First, heavy minerals other than zircon and tourmaline were probably rare in the sedimentary part of the source area. Second, other heavy minerals, such as hornblende and garnet, are less stable during transport and burial than are zircon and tourmaline, so any of these minerals that were derived from the source area did not survive.

Muscovite is present in volumes of less than 0.5 percent, and it occurs primarily in the finer grained samples. Coalified wood is a common constituent in some samples (tables 5 through 14); the wood was derived locally and redeposited with the sand.

Invertebrate fossils were also derived locally and incorporated into sandstones that overlie fossiliferous limestones near the top of the Travis Peak Formation. Fragments of oysters, ostracods, and echinoids are evidence of a normal-marine depositional environment for the limestone (D. Bebout, personal communication, 1985).

Matrix

Detrital clay matrix was deposited with some of the Travis Peak sandstones. Where detrital grains of sand-sized clay clasts could be recognized, they were counted separately from clay matrix (tables 5 through 14). However, where clay clasts were deformed by compaction and are no longer recognizable as distinct grains, they were counted as matrix (clay-sized fines). X-ray diffraction analysis of detrital clay matrix in the less than 5-μm-size fraction has been performed on samples from the Clayton Williams Sam Hughes No. 1, ARCO Phillips No. 1, Ashland S.F.O.T. No. 1, and Prairie Mast No. 1-A cores. Illite and chlorite are the most abundant detrital clay minerals (David K. Davies and Associates, 1984a, 1984b, 1985a, 1985b). Detrital kaolinite occurs in only two samples from the ARCO Phillips No. 1 well, and mixed-layer illite-smectite with approximately 5 percent smectite layers occurs in the Ashland S.F.O.T. No. 1 core and in trace amounts in the Prairie Mast No. 1-A core.

A few zones near the top of the Travis Peak are sandy limestones in which the matrix is fine-grained carbonate mud. Some mud remains calcite, but much of it has been dolomitized or ankeritized.

Porosity

The amount of porosity in Travis Peak sandstones is quite variable, ranging from 0 to 22 percent measured in thin section (tables 5 through 14). Thin-section porosity was divided into primary and secondary types; secondary porosity results from dissolution of framework grains or cements. Average primary porosity recognized in thin section is 0.65

percent (standard deviation = 1.2 percent), whereas secondary porosity averages 1.9 percent (standard deviation = 2.4 percent). The low volume of primary porosity suggests that most original depositional porosity in the sandstones was destroyed by compaction and cementation, and that much of the remaining porosity of the Travis Peak results from mineral dissolution.

Porosity was also measured in a porosimeter, which determines effective pore volume using the principle of Boyle's Gas Law. The correlation of thin-section porosity with porosimeter porosity is .28 for all samples. Much of the difference between values of porosity that can be observed in thin section and porosimeter-measured porosity is the presence of abundant microporosity between authigenic clay crystals and in clay matrix. A smaller source of error is secondary porosity within leached feldspar grains. In matrix-free sandstones, the correlation between porosimeter and thin-section porosity is .42, which is significant at the .001 level.

There is a significant trend of decreasing porosimeter porosity with depth below the top of the Travis Peak (fig. 5); both the mean porosity at any given depth and the range of observed porosities decrease. Primary and secondary porosity measured in thin section also decrease with depth below the top of the Travis Peak. The mean value of primary porosity exhibits little change with depth (fig. 6), but the range of primary porosity values decreases. Thus, several samples near the top of the Travis Peak have high values of primary porosity, but the values are uniformly low deeper in the formation (fig. 6). In constrast, secondary porosity decreases significantly with depth in the Travis Peak both in mean value and in the range of porosities present (fig. 7).

In clean, well-sorted sandstones, the depositional porosity was probably quite high, perhaps as much as 45 percent (Jonas and McBride, 1977). Porosity was probably reduced to 35 percent during the first few feet of burial (Jonas and McBride, 1977), after which compaction and grain reorientation associated with deeper burial reduced the porosity to an average of about 27 percent. Few ductile grains are present in the Travis Peak

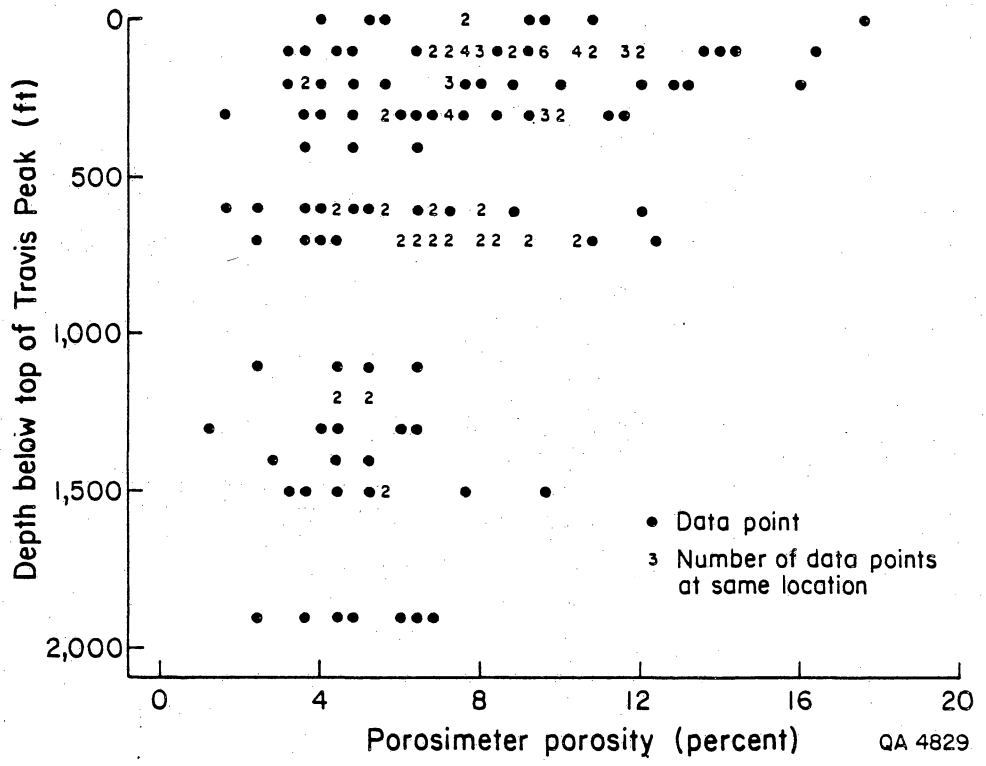

Figure 5. Porosimeter-measured porosity decreases with depth below the top of the Travis Peak.

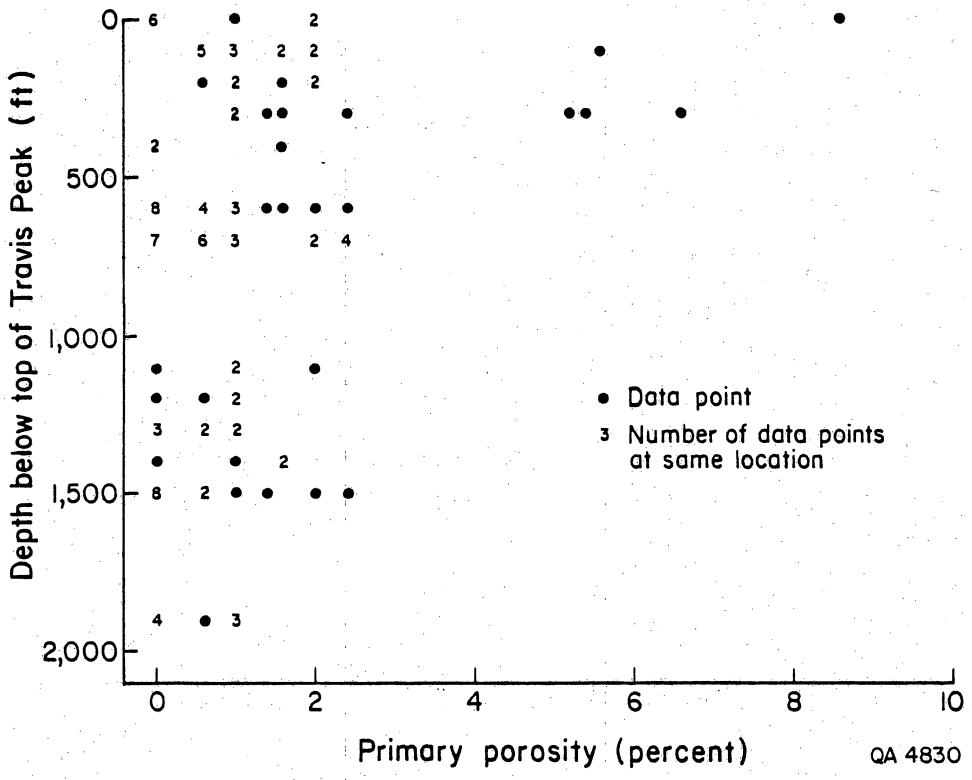

Figure 6. Primary porosity measured in thin section decreases with depth below the top of the Travis Peak.

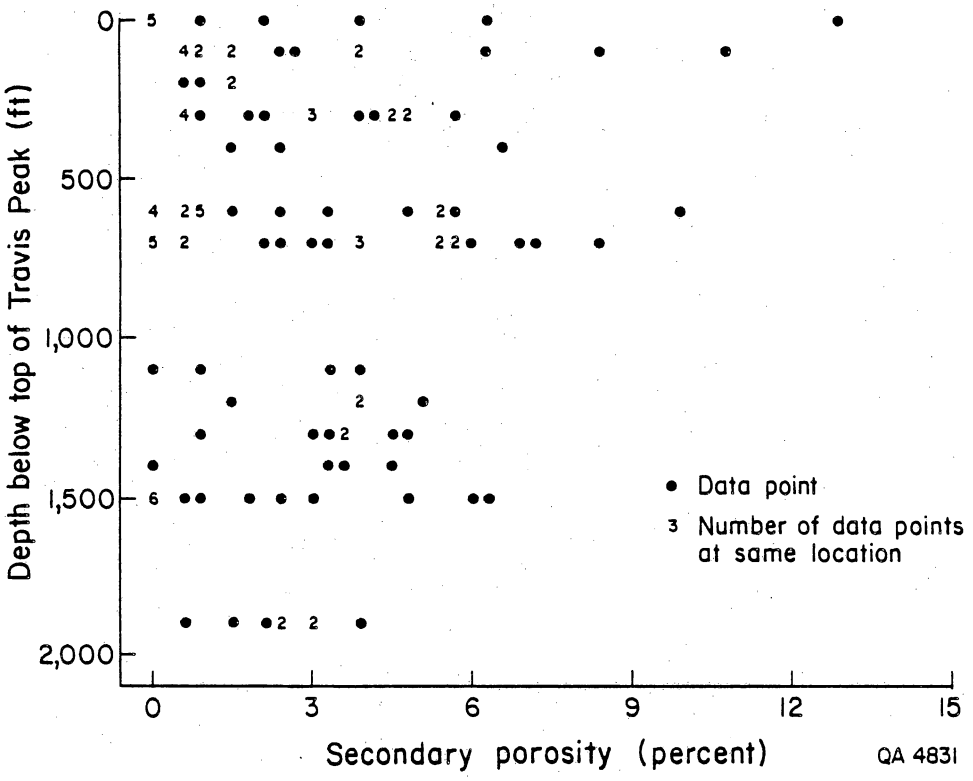

Figure 7. Secondary porosity measured in thin section decreases with depth below the top of the Travis Peak.

sandstones, so that compaction by deformation of ductile grains was probably minor except in intervals with abundant clay clasts. The pre-cement porosity, which is calculated by adding the total volume of cement to the volume of primary porosity, is a measure of the amount of primary porosity that remained after compaction and before cementation. The average pre-cement porosity in matrix-free sandstones is 26.7 percent (standard deviation = 5.2 percent). The average volume of total authigenic cements, including reservoir bitumen, in matrix-free sandstones is 25.8 percent (standard deviation = 5.3 percent). In most samples, therefore, the primary porosity that remained after compaction was almost completely occluded by authigenic minerals. Some samples of matrix-free sandstones contain as much as 40 percent cement. It is unlikely that 35 to 40 percent primary porosity could have remained after burial compaction; to contain 35 to 40 percent cement, these samples must have undergone some dissolution of framework grains.

Cements/Authigenic Minerals

Authigenic minerals constitute between 0 and 52 percent of the sandstone volume in the Travis Peak samples. The volume of rock made of authigenic cement is normally distributed with an average of 23.0 percent and standard deviation of 7.8 percent. The most important control on the total volume of cement in the sandstones is the amount of detrital matrix; the correlation coefficient between matrix and total cement is -0.64. Large amounts of detrital matrix must have lowered the permeability of the sediment, such that a smaller volume of mineralizing fluids passed through matrix-rich sandstones compared to clean sandstones. Furthermore, abundant detrital matrix probably reduced the availibility of nucleation sites on detrital grains, and in particular inhibited the precipitation of quartz cement. There is not a significant correlation of total cement with absolute depth or depth below the top of the Travis Peak.

There are several authigenic phases in the Travis Peak sandstones; authigenic quartz, illite, chlorite, ankerite, and dolomite are the most abundant (tables 5 through 14). Less

common authigenic minerals include calcite and iron-rich calcite, feldspar overgrowths, pyrite, barite, and anhydrite. In addition, solid hydrocarbons occur in all cores except the Amoco Kangerga "C" No. 1. The solid hydrocarbon material, also known as reservoir bitumen, was considered a cement.

Authigenic Quartz

Authigenic quartz is the most abundant cement in the Travis Peak, with an average volume of 15.5 percent (standard deviation = 6.7 percent). In samples with no detrital clay matrix, the average volume of quartz cement is 18.4 percent (standard deviation = 4.3 percent). In zones with abundant quartz cement, the overgrowths completely occlude primary porosity and form an interlocking mesh of quartz crystals (pls. IA and IVA). In zones with less authigenic quartz the overgrowths do not grow together, thus some primary porosity remains between crystal faces (pls. IC, D, and IVA). Euhedral crystals characterize the zones of clean sandstone and less abundant quartz cement (pls. IC and IVB). Rare intervals of high permeability in the Travis Peak correspond to these zones of clean sandstone with relatively low volumes of quartz cement. For example, permeable zones in the Clayton Williams Sam Hughes No. 1 well (6,843 ft; pl. IC) and the ARCO Phillips No. 1 well (8,216 and 8,246 ft; pl. IVA) have average unstressed permeability of 30 md, which is several orders of magnitude greater than the average permeability in the Travis Peak.

The relation between the volume of quartz cement in matrix-free sandstones and permeability is not as straightforward as might be expected. In the ARCO Phillips No. 1 core there is a significant inverse relation between quartz cement and log stressed permeability (correlation coefficient = -.73). The Clayton Williams Sam Hughes No. 1 core has a relatively high correlation coefficient (-.51) between quartz cement and log unstressed permeability, but because the sample size is small, it is not statistically significant. However, in the Ashland S.F.O.T. No. 1 and the Prairie Mast No. 1-A cores no significant trend of quartz cement versus permeability exists. Furthermore, when data

from all ten wells are considered, there is no significant correlation of quartz cement and permeability either in all samples or in matrix-free samples. The significant inverse correlation of quartz cement with permeability in matrix-free samples in the ARCO Phillips No. 1 probably occurs because this well contains zones with relatively high permeability and a relatively low volume of quartz cement. Matrix-free samples from the Ashland S.F.O.T. No. 1 and Prairie Mast No. 1 cores, on the other hand, have varying amounts of quartz cement, but their permeability is uniformly low. The fact that matrix-free samples with low quartz volumes have low permeability implies that other cements are abundant in those samples and control permeability.

Authigenic Clay Minerals

Authigenic clays that have been identified in the Travis Peak sandstones are illite, chlorite, kaolinite, and mixed-layer illite-smectite. Authigenic clays average 2.6 percent of the sandstone volume, although much of that volume is actually microporosity. In thin sections, microporosity cannot be distinguished from clay flakes, but by SEM it can be seen that abundant porosity occurs between individual clay flakes (pl. IVC, D). Illite and chlorite are by far the most abundant authigenic clays. In matrix-free sandstones their combined average volume is 3.0 percent (standard deviation = 2.3 percent). Kaolinite was observed in thin section only in the Amoco Kangerga "C" No. 1 core, where it commonly appeared to be engulfed in quartz overgrowths. Rare kaolinite books were identified by SEM in one sample from 8,246 ft in the ARCO Phillips No. 1 core. Mixed-layer illite-smectite with approximately 5 percent smectite layers was identified by X-ray diffraction in clean sandstones in the Ashland S.F.O.T. No. 1 core (David K. Davies and Associates, 1985a). A trace of mixed-layer illite-smectite occurred in one sandstone sample from the Prairie Mast No. 1-A core (David K. Davies and Associates, 1985b).

Illite occurs as thin rims of tangentially oriented crystals that coat detrital grains (pl. VA). Where the rims are sufficiently thick, they prevented nucleation of quartz

overgrowths. Small quartz crystals nucleated on grains with breaks in the illite rims (pl. VA). Where illite rims were thin, quartz cement precipitated over them, and the illite rim now forms a distinct boundary between detrital grain and overgrowth. Illite also occurs as delicate fibers and compact flakes inside primary and secondary pores (pl. IVC). In particular, secondary pores associated with dissolved feldspar grains commonly contain illite fibers (pl. VB).

Chlorite occurs as individual flakes and rosettes inside primary and secondary pores (pls. IIA and IVD). Like illite, abundant microporosity occurs between chlorite crystals. Both illite and chlorite in the Travis Peak are iron rich (David K. Davies and Associates, 1984a, 1984b, 1985a, 1985b). The total authigenic clay content in all matrix-free sandstones does not have a significant correlation with either stressed or unstressed permeability.

Authigenic Carbonate Cements

Dolomite (pl. IIB), ankerite (pls. IIC and VC), calcite, and iron-rich calcite cements all occur in the Travis Peak samples, but only dolomite and ankerite are common (tables 5 through 14). Calcite and iron-rich calcite were observed only in the ARCO Phillips No. 1 core in sandstones above or below limestone beds. Fossils and carbonate mud in the adjacent limestones probably provided the source of $CaCO_3$ for the calcite cement. Dolomite cement is more common, with an average volume of 1.1 percent in the Travis Peak samples (standard deviation = 3.2 percent). Most samples contain a trace to one percent dolomite, but a few samples are heavily dolomitized (up to 34 percent) (tables 5 through 14). Dolomite rhombs commonly have ankerite rims (pl. IIB). Dolomite is most abundant in the delta-fringe facies at the top of the Travis Peak. In the delta-fringe facies of the Ashland S.F.O.T. No. 1 well, dolomite and ankerite rhombs occur preferentially along ripple faces (pl. IID) where they replace detrital grains, particularly clay clasts. In other samples dolomite rhombs commonly occur within detrital matrix or zones of

abundant clay clasts. Samples from the deeper, fluvial sections of the Travis Peak contain little or no dolomite (tables 7 and 8).

Similarly, ankerite is also most abundant near the top of the Travis Peak (fig. 8). At any given depth there is a range of ankerite volumes (average ankerite volume = 2.2 percent, standard deviation = 3.3 percent), but the maximum amount of ankerite present decreases with depth below the top of the Travis Peak. Therefore, ankerite is most abundant in the marine-associated delta-fringe facies, and its abundance decreases with depth into the fluvial section. Where ankerite is present in large volumes the permeability is uniformly low, but at small volumes of ankerite, permeability has a wide range (fig. 9). Ankerite content in large volumes is probably an important control on permeability, but in low volumes other factors control permeability.

Petrographic relationships show that ankerite cement precipitated after quartz overgrowths (pl. IIC). In places, ankerite replaced framework grains and earlier cements.

Feldspar

Albite overgrowths on plagioclase grains are present in most samples, but in volumes less than 0.5 percent. Albite overgrowths commonly occur on partially dissolved plagioclase grains that now appear to be in the process of being redeposited (pl. VD). The diagenetic history of these grains was probably as follows: (1) partial dissolution, (2) albitization of the remaining detrital plagioclase, and (3) precipitation of euhedral overgrowths on sites within the leached grain. This process was described by Gold (1984) for plagioclase in Miocene sandstones of the Louisiana Gulf Coast. The small crystals that grow within the leached grains are not in exact optical continuity with each other, thus in thin section the extinction pattern shows patchy zones or "chessboard" twinning (Gold, 1984).

Feldspars from six Travis Peak samples have been analyzed by an electron microprobe to determine the major element composition. Plagioclase composition ranges from

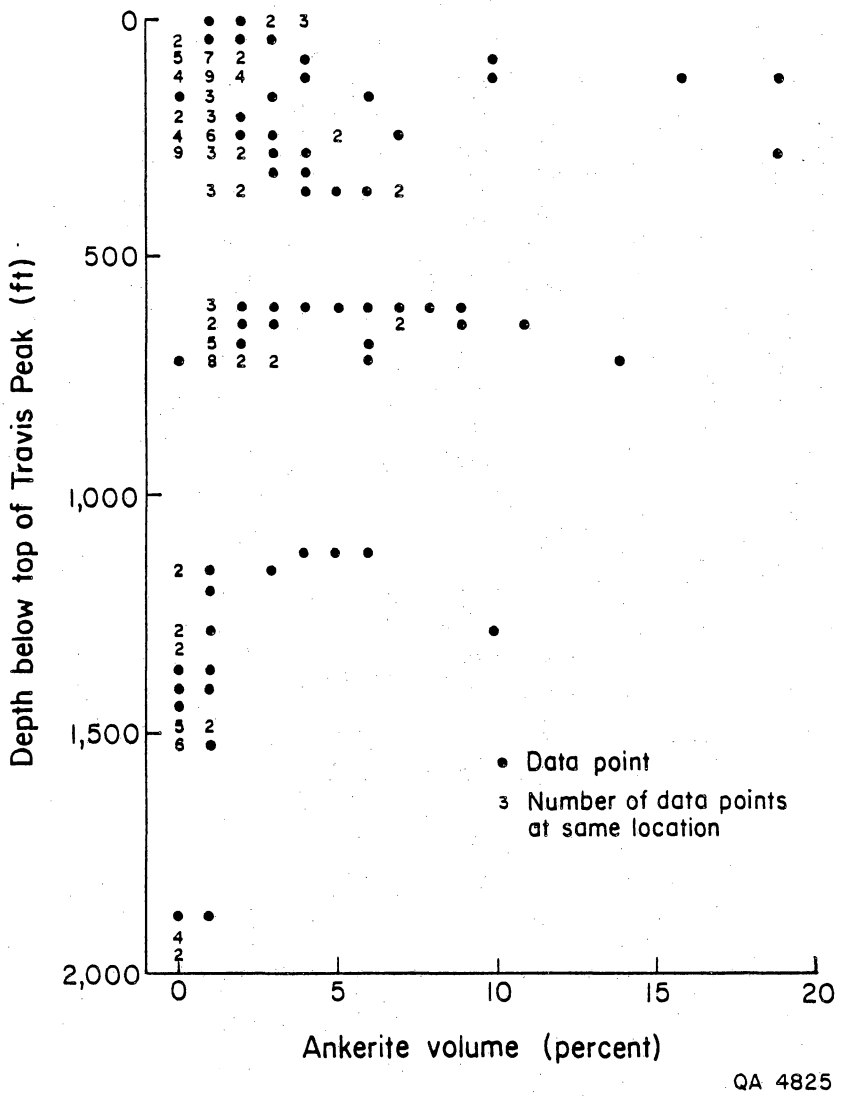

Figure 8. Ankerite volume decreases with depth below the top of the Travis Peak.

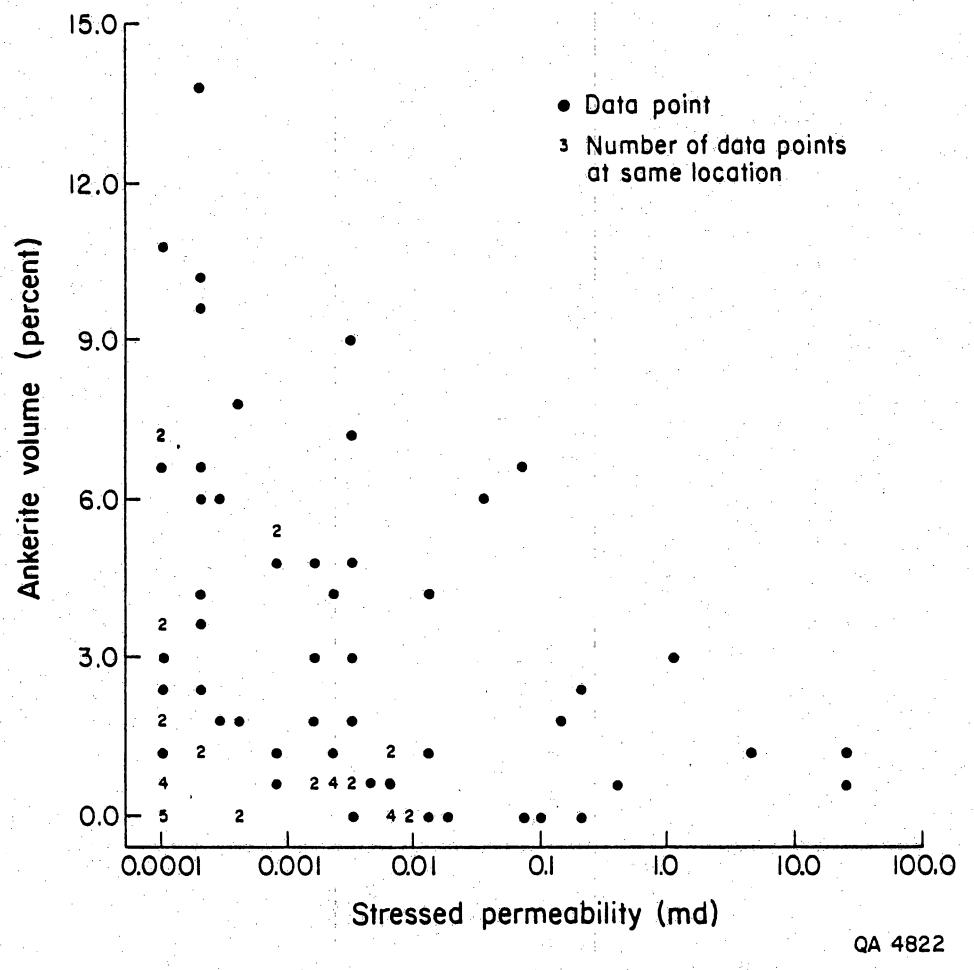

Figure 9. Inverse relationship between ankerite volume and permeability measured under in situ conditions.

$An_{0.1}$ to An_{19}, but 65 percent of the analyses were less than An_2 and 87 percent were less than An_5. ("An" is the average anorthite content of the plagioclase in mole percent.) Feldspars with chessboard twinning consistently have compositions less than An_2. Feldspars that retain more calcium (greater than An_{10}) represent a variety of grain types, including grains with distinct albite twinning, untwinned grains, and extensively dissolved grains. However, other examples of each of these grain types have compositions of less than An_2. Therefore, only grains with chessboard twinning are consistently associated with albite composition of less than An_2.

The microprobe analyses indicate that plagioclase in the Travis Peak has been extensively albitized. The original detrital composition of the plagioclase is not known, but it was probably more calcic than it is now, possibly in the range An_{10} to An_{50}. The presence of plagioclase with An_{20} in the Travis Peak indicates the source area contained feldspars at least as calcic as oligoclase. Medium-grade metamorphic rocks and igneous diorites and granodiorites in the source area could have contributed both oligoclase (An_{10} to An_{30}) and andesine (An_{30} to An_{50}). It seems probable that the Travis Peak feldspars were albitized after burial, and the albite is therefore not detrital. Many of the Travis Peak plagioclase grains are extensively leached and would not have survived transport in such a condition, indicating they have been dissolved since burial. Similarly, the precipitation of internal overgrowths within partially leached grains must have occurred since burial and dissolution of the feldspars. Therefore, it seems likely that albitization has occurred since burial. However, it is possible that some fraction of the albite in the Travis Peak was inherited from older, albitized sandstones or from low-grade metamorphic rocks in the source area.

The geochemical conditions in the Travis Peak favor the formation of albite from more calcic plagioclase. Fluids in the Travis Peak are sodium-calcium-chloride brine (Kreitler and others, 1983), and the high amount of sodium should cause albitization of feldspars at the temperatures measured in these wells. Bottom-hole temperature in the

Clayton Williams Sam Hughes No. 1 well is 204°F, uncorrected, at 7,200 ft, and 220°F, uncorrected, in the Ashland S.F.O.T. No. 1 well at 10,400 ft.

In addition to dissolution and albitization of plagioclase, dissolution of orthoclase apparently took place during burial diagenesis. Partially dissolved orthoclase was observed in the Ashland S.F.O.T. No. 1 and Prairie Mast No. 1-A cores. Orthoclase is relatively common in the upper sections of the Prairie Mast No. 1-A core, but it is absent in the deepest section of core from 9,900 ft (table 8). No orthoclase was observed in any cores from more than 1,300 ft below the top of the Travis Peak (fig. 10). Absolute depth of the core does not seem to be as important in determining orthoclase content as is the stratigraphic position within the Travis Peak. Samples from the Ashland S.F.O.T. No. 1 core from 10,100 ft contain orthoclase, but these samples are within the delta-fringe facies and are only about 700 ft below the top of the formation.

Orthoclase content is low at the top of the Travis Peak (fig. 10), so selective orthoclase dissolution may also have occurred there. Thus, dissolution of orthoclase may explain the particularly high values of secondary porosity at the top of the formation (fig. 7).

Other Authigenic Minerals

Pyrite, barite, and anhydrite are the other authigenic mineral phases that were observed in the Travis Peak. Minor anhydrite cement was identified in thin sections from six of the ten wells; most samples contain either no anhydrite or less than one percent, but one sample from the Prairie Mast No. 1-A core (9,212 ft) has 9 percent anhydrite cement (tables 5 through 14). Anhydrite replaces both framework grains and cements (pl. IIIA); petrographic evidence indicates it precipitated after quartz overgrowths.

Barite is even less abundant than anhydrite, with a maximum volume of 0.5 percent in a few wells. In most thin sections no barite cement was counted. Bladed barite crystals occur in secondary pores, indicating they were a relatively late-stage cement.

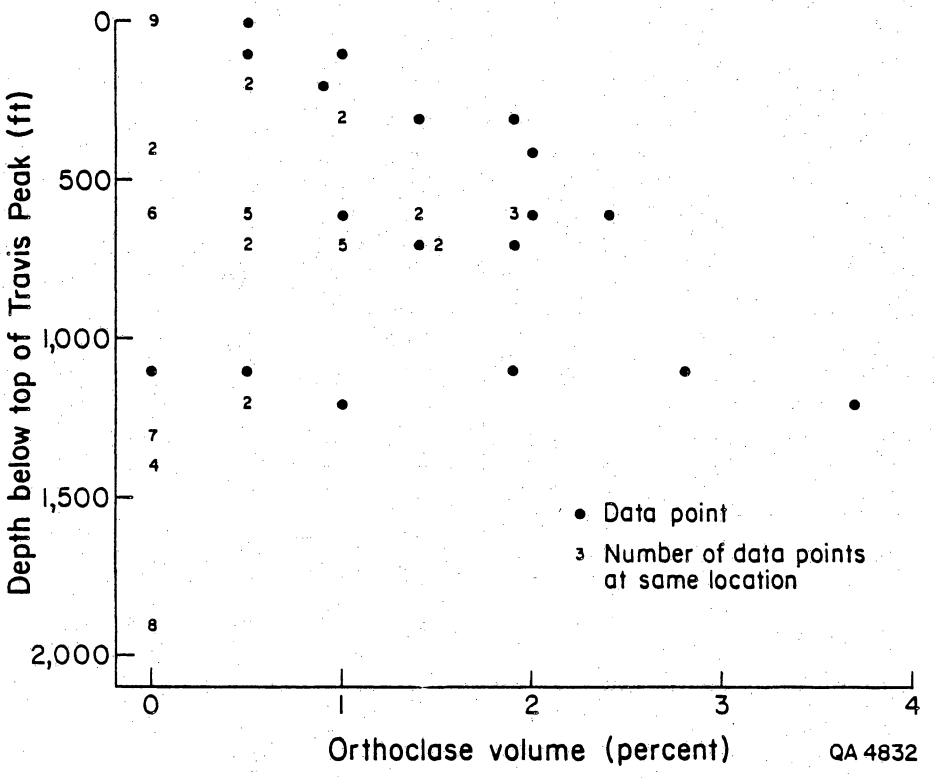

Figure 10. Distribution of orthoclase with depth below the top of the Travis Peak.

Pyrite is present in small amounts in most cores, but it is particularly abundant in the Ashland S.F.O.T. No. 1 (table 7), Prairie Mast No. 1-A (table 8), and Stallworth Everett "B" No. 2 cores (table 12). Much of the pyrite is associated with coalified wood fragments. Pyrite nodules in the Prairie Mast No. 1-A core (pl. IIIB) extensively replace framework grains and quartz cement.

Solid Hydrocarbons

Solid hydrocarbon accumulations that line pores in some sandstones (pl. IIIC) were observed in all cores except the Amoco Kangerga "C" No. 1 (tables 5 through 14). This material is interpreted to be reservoir bitumen, which was defined by Rogers and others (1974) as "black, solid graphitic, or asphaltic particles or coatings within the porosity of oil- and gas-bearing reservoirs." The reservoir bitumen occurs primarily within the delta-fringe facies and is most abundant in the upper 300 ft of the Travis Peak Formation (fig. 11, tables 5 through 14). Wells with thick delta-fringe facies, such as the Ashland S.F.O.T. No. 1 and Prairie Mast No. 1-A, contain only minor amounts of reservoir bitumen in the deepest part of the delta-fringe facies, 600 to 700 ft below the top of the Travis Peak (tables 7 and 8).

The reservoir bitumen fills primary pores and commonly coats quartz overgrowths (pl. IIID), indicating it entered the pores during burial diagenesis. The emplacement of bitumen appears to have been a late diagenetic event that occurred after both quartz and ankerite precipitation. The volume of reservoir bitumen is as high as 19 percent in a sample from 8,232 ft in the Stallworth Renfro No. 2 well (table 10). The average volume is 1.5 percent (standard deviation = 3.6 percent), but the distribution is not normal because most samples do not contain any reservoir bitumen. Among samples that contain reservoir bitumen, the average volume is 5.6 percent (standard deviation = 5.5 percent). Where reservoir bitumen is abundant, it drastically reduces porosity. For example, in the ARCO Phillips No. 1 core, a sample from 8,246.1 ft has thin-section porosity of 8.4 percent and no

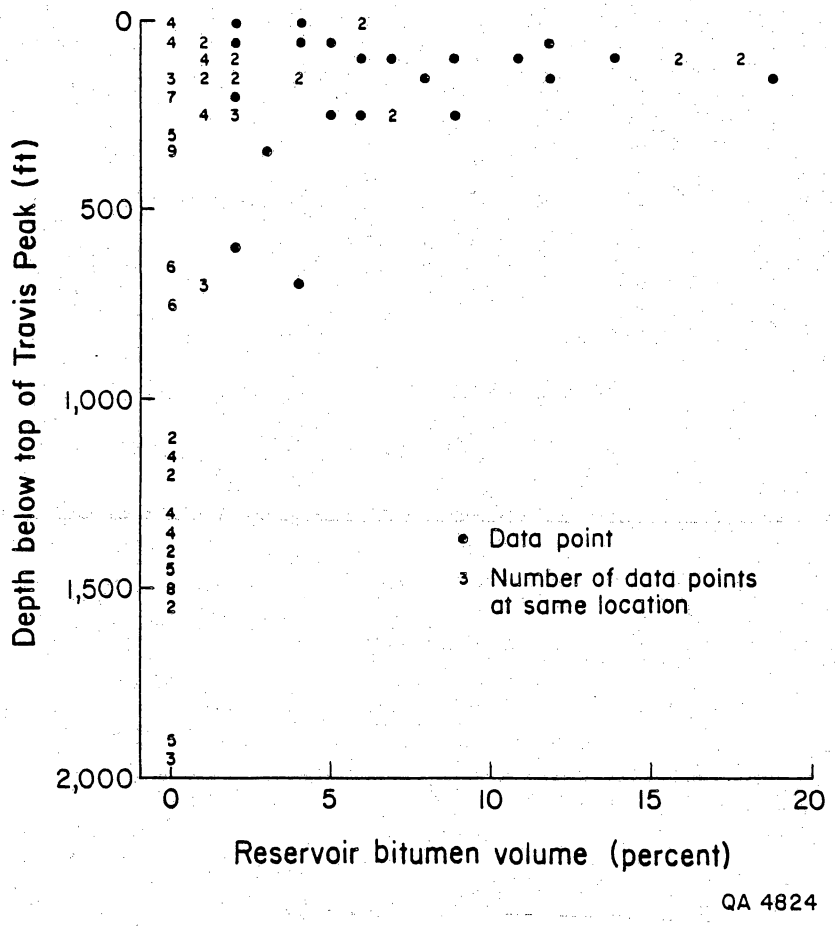

Figure 11. Reservoir bitumen decreases with depth below the top of the Travis Peak.

bitumen. In contrast, a sample from 8,246.8 ft contains 9.2 percent reservoir bitumen and no thin-section porosity.

Samples that contain large amounts of reservoir bitumen, for example greater than 10 percent, probably underwent some dissolution of framework grains and cements before or during the emplacement of reservoir bitumen in the sandstones. It is unlikely that the Stallworth Renfro No. 2 sample from 8,232 ft retained 19 percent open porosity late in the diagenetic sequence when the reservoir bitumen was emplaced; this sandstone also contains 21 percent of other authigenic cements. A total of 40 percent by volume of mineral cements and reservoir bitumen is not a realistic figure for pre-cement porosity. Therefore, there must have been dissolution of framework grains or cements or both to create pore space for such a large volume of reservoir bitumen late in the diagenetic history. This conclusion is supported by the relatively low volume of detrital quartz in this sample, only 56.4 percent compared to an average for all wells of 65.4 percent. The dissolution may have been caused or enhanced by the emplacement of organic acids associated with these organic molecules within the sandstones (Surdam and others, 1984).

Within the delta-fringe facies, permeability differences apparently controlled the distribution of reservoir bitumen. Intervals of well-sorted, rippled and crossbedded sandstones now contain the most reservoir bitumen. Burrowed and other poorly sorted sandstones contain little or no reservoir bitumen. Therefore, many zones that originally had relatively high porosity and permeability may now be tight because of reservoir bitumen.

Elemental analysis was performed on four samples of the solid, black reservoir bitumen from sandstones in the Delta Williams "A" No. 1 (8,190 ft), Sun Janie Davis No. 2 (7,493 ft), Stallworth Renfro No. 2 (8,232 ft), and Stallworth Everett No. 2 (8,318 ft) cores. The hydrogen/carbon (H/C) ratio of the reservoir bitumen varies from 0.79 to 0.90. An H/C ratio greater than 0.58 suggests that this reservoir bitumen formed by deasphalting of pooled oil after solution of large amounts of gas (C_1 to C_6) into the oil (Rogers and others,

1974). When gas went into solution in the accumulated oil, it lowered the solubility of heavy molecules such as aromatics and asphaltenes, causing them to precipitate (Tissot and Welte, 1978). After precipitation, the reservoir bitumen may have continued to evolve to lower H/C ratios by polymerization and cross-linking, resulting in a more insoluble, carbon-rich material than the originally precipitated asphaltenes. Sulfur, common in reservoir bitumens, apparently promotes cross-linking (Rogers and others, 1974).

The gas that caused deasphalting was either generated from the pooled oil by thermal alteration, or it was injected from outside by a second migration of gas into the reservoir. Gas may have been generated in deeper, downdip parts of the stratigraphic section and then migrated updip, causing deasphalting in oil reservoirs located along the gas migration path.

Additional geochemical analyses may permit differentiation between the processes of gas generation by thermal alteration and by secondary gas migration. Evaluating the maturation level of kerogen in shales adjacent to the bitumen-bearing sandstones will establish if rocks at that depth have undergone sufficient maturation to cause thermal alteration and gas generation. If the maturation level of the adjacent shales is not high, it would suggest that the gas came from a second phase of hydrocarbon migration from deeper in the basin. In addition, comparison of the carbon isotopes in reservoir bitumen with carbon isotopes in oil from the Travis Peak may distinguish between deasphalting and thermal alteration. Deasphalting results in similar carbon isotopes in the reservoir bitumen and the original oil, but thermal alteration results in isotopically heavy carbon in the residue and isotopically light carbon in the methane that is generated.

The presence of reservoir bitumens in what were originally the more porous and permeable sandstones is explained by the mechanism of deasphalting by gas solution. The oil from which the asphaltenes precipitated migrated into the good reservoir facies, but it did not migrate into the less permeable, poorly sorted sandstones. Thus, the presence of reservoir bitumen may provide a clear picture of where oil occurs within a reservoir.

PERMEABILITY

Permeability of the Travis Peak sandstones was measured in two ways. All samples were measured at surface pressure conditions (200 psi); these measurements are referred to as unstressed permeability. Most samples from the four GRI cooperative wells were also measured under in situ conditions of overburden pressure; these measurements are referred to as stressed permeability. The correlation between permeability and porosimeter porosity is high, so porosimeter porosity is a good predictor of permeability. The correlation coefficient of porosimeter porosity versus log unstressed permeability is 0.64; correlation with log stressed permeability is 0.70.

The correlations between permeability and various individual cements (quartz, ankerite, total authigenic clay, and reservoir bitumen) are not statistically significant. However, the correlation of total cement in matrix-free sandstones with log unstressed permeability (fig. 12) is significant at the .001 level. Therefore, from thin-section data the best predictor of permeability in clean sandstones is the total volume of authigenic cement, including reservoir bitumen. Individual cements, even quartz, are less useful as predictors of permeability, because even if one cement has low volume in a given sample, other cements may be abundant and act as the control on permeability.

Permeability decreases with depth below the top of the Travis Peak (fig.13). With the exception of one sample from the Prairie Mast No. 1-A core at 9,959 ft, only samples within about 200 ft of the top of the Travis Peak have stressed permeabilities greater than 0.1 md. Samples within 200 ft of the top of the Travis Peak have a wide range of stressed permeabilities, from less than .0001 md to more than 90 md. Deeper in the formation permeability decreases, and most samples range from less than .0001 md to .1 md (fig. 13). Therefore, the diagenetic processes that caused extensive cementation and resulting low permeability throughout most of the Travis Peak Formation may not have operated as completely on the sediments deposited near the top of the Travis Peak. These deposits

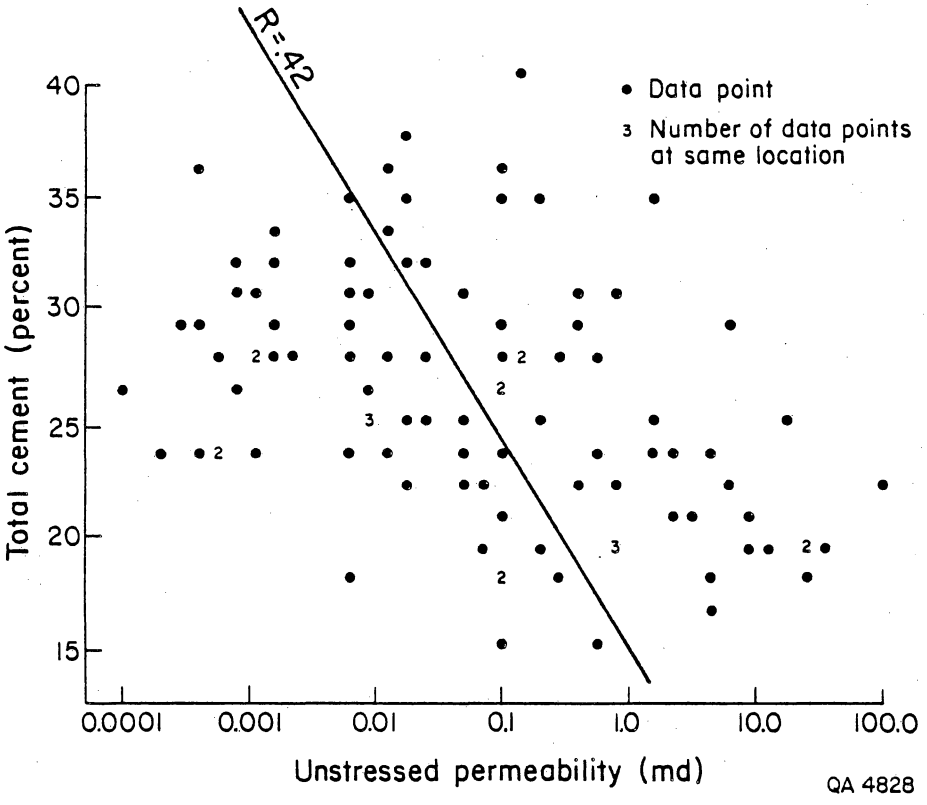

Figure 12. Inverse relationship between total cement volume and conventionally measured permeability.

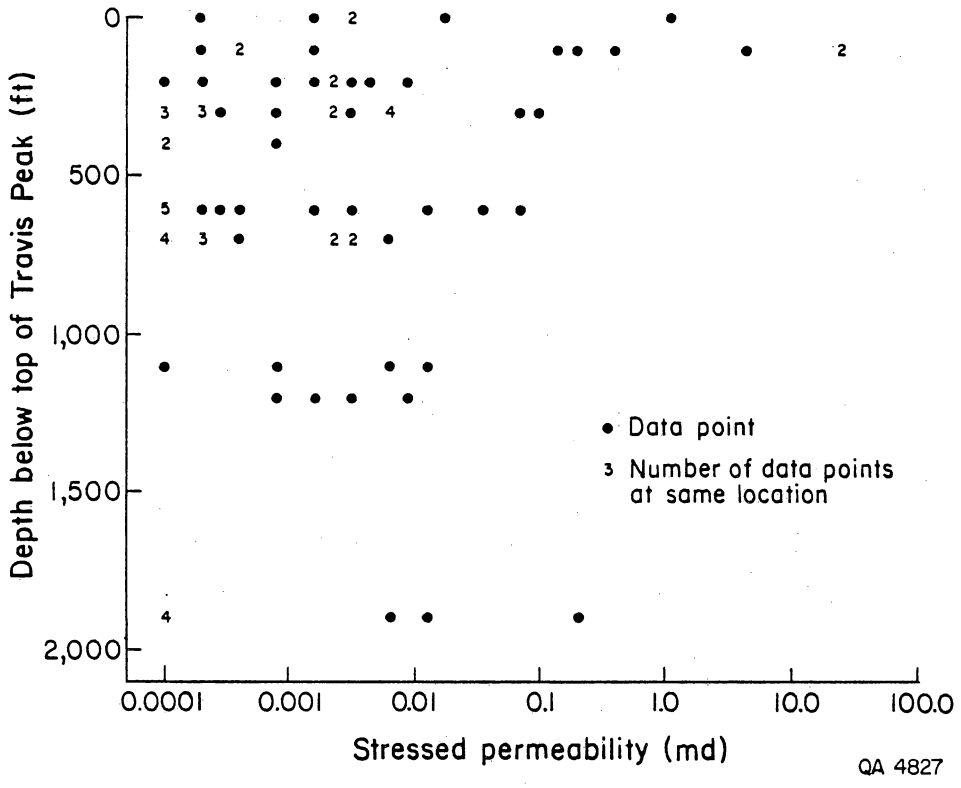

Figure 13. Permeability measured under in situ conditions decreases with depth below the top of the Travis Peak.

retain some primary porosity, and, therefore, higher permeability than the rest of the formation. In addition, processes that caused dissolution of framework grains and generation of secondary porosity may have been more active on deposits near the top of the Travis Peak. Additional geochemical work on the authigenic cements, including determination of their isotopic composition, will provide more information about the temperature and fluid conditions under which the cements precipitated. This additional information should make it possible to determine why some aspects of the diagenesis near the top of the Travis Peak differed from diagenesis in the rest of the formation.

SUMMARY AND DIAGENETIC HISTORY

Petrographic relations of the authigenic cements in the Travis Peak sandstones can be used to determine the order in which the cements precipitated. The earliest cements to form were clays that coated detrital grains with tangentially oriented crystals, primarily illite. The clay coats are probably authigenic, although some of the coats could have formed by infiltration of clays into the sandstones after deposition as vadose water percolated down to the water table (Wilson and Pittman, 1977).

Extensive quartz overgrowths, the next cement to precipitate, covered thin clay coats and sharply reduced primary porosity. The amount of quartz cement in the Travis Peak sandstones indicates that large volumes of water must have moved through these deposits at some time in their burial history to account for the volumes of silica that were deposited as cements. Possible sources of water include (1) meteoric water that recharged in a highland area and flowed through the sandstones during shallow burial, (2) fluids derived from basin compaction, or (3) fluids that moved by thermally driven free convection and were recycled through the sandstones during deeper burial. Some of the silica in the quartz overgrowths could have been derived from pressure solution of detrital quartz grains. However, the amount of pressure solution and stylolites observed in thin

sections was minor, so this source probably was sufficient to provide only a relatively small volume of the observed quartz cement. Furthermore, it is likely that much of the pressure solution occurred after quartz cementation because stylolites cut both detrital grains and overgrowths. Finally, the relatively high amount of pre-cement porosity suggests that quartz cementation began early in the burial history, probably at depths too shallow for pressure solution to have begun. Isotopic analysis of quartz overgrowths, which will be conducted on a variety of Travis Peak samples, should provide information on the type of fluid that precipitated the cement and when in the burial history the cement formed.

Ankerite was the next major authigenic mineral to precipitate after quartz. It probably formed as a late-stage cement during deep burial of the sandstones. The iron and magnesium in the ankerite may have been derived from mixed-layer illite-smectite during illitization of iron- and magnesium-bearing smectite layers. Much of the ankerite is associated with dolomite; commonly, carbonate rhombs are dolomitic in the center and contain ankerite around the crystal margins. Perhaps carbonate precipitation began before iron was available, therefore dolomite formed. As the subsurface fluids evolved to a more iron-rich composition, ankerite precipitation became prevalent. Some of the dolomite may have been an early cement that precipitated during shallow burial, with magnesium derived from seawater. Early dolomite may also have served as a nucleus around which later ankerite precipitated.

Dissolution of feldspars and precipitation of authigenic chlorite and illite (both types of clay are iron rich, according to David K. Davies and Associates, 1984a, 1984b, 1985a, 1985b) were also relatively late diagenetic reactions that occurred at approximately the same time as ankerite precipitation. Production of CO_2 by decarboxylation reactions during organic maturation may have driven the feldspar dissolution reaction. The volume of organic matter in Travis Peak shales is probably large in comparison to the amount of feldspar in Travis Peak sandstones; thus CO_2 production from organic reactions is most likely sufficient to account for all the secondary porosity in the Travis Peak. Precipitation

of iron-rich illite and chlorite was probably related to the other late-stage reactions, with their iron and magnesium derived from the smectite to illite transformation that supplied iron and magnesium for ankerite. In addition, the silica in the authigenic clays may have been supplied by dissolution of both plagioclase and orthoclase feldspars. The authigenic clays commonly occur within secondary pores associated with leached feldspars. Dissolution of orthoclase is also the most likely source of potassium in the authigenic illite. Thus, the reactions for organic maturation, feldspar dissolution, and ankerite, illite, and chlorite precipitation are interrelated and all probably occurred at approximately the same time.

Migration of liquid oil into the Travis Peak sandstones followed ankerite precipitation. At a later time gas entered the accumulated oil and caused precipitation of reservoir bitumens, which occluded much of the remaining porosity in some zones near the top of the Travis Peak. The concentration of reservoir bitumen near the top of the formation was probably caused by one of the following possibilities: (1) The lower, sand-rich part of the Travis Peak lacks traps and seals, so oil that entered the lower part of the formation continued to migrate upward through the sandstones until it was trapped near the top of the Travis Peak. Thicker shale beds of the upper Travis Peak or the overlying Sligo Formation may have acted to seal hydrocarbons in the upper Travis Peak. (2) The lower part of the Travis Peak has a smaller range of permeabilities than the upper Travis Peak, and most samples have less than .1 md permeability. Because of the low permeability, liquid oil may not have migrated into or through the lower Travis Peak sandstones from the source rocks. The most probable source beds for the Travis Peak hydrocarbons are either Travis Peak marine shales that were deposited downdip from the fluvial-deltaic sandstones (fig. 2) or Jurassic shales. Hydrocarbons generated in these parts of the stratigraphic section may have moved updip directly into the sandstones in the upper Travis Peak.

Some of the late diagenetic reactions continued after the reservoir bitumen was emplaced. There are some secondary pores that lack reservoir bitumen in samples that are otherwise completely filled with bitumen. It is likely that additional feldspar dissolution

occurred in these samples after the emplacement of the reservoir bitumen. Late feldspar dissolution indicates that gas generation continued even after the initial formation of gas that caused the precipitation of the asphaltenes from the liquid oil. Gas generation, feldspar dissolution, and albitization may be continuing today.

Future work on Travis Peak sandstones will be designed to answer several questions that have been raised by the initial petrographic studies. Additional organic geochemical studies should help determine the origin of the reservoir bitumen and the relative timing of emplacement of the bitumen compared to precipitation of authigenic minerals. Evaluation by vitrinite reflectance and pyrolysis of thermal maturity of shales interbedded with the bitumen-bearing sandstones should provide information necessary to determine if the gas that caused precipitation of the reservoir bitumen was derived from Travis Peak oil or from a secondary migration of hydrocarbons into the formation.

Geochemical work on the various authigenic cements will include identification of the oxygen isotopic composition of quartz cement to determine the temperature and composition of the fluid that precipitated the abundant quartz overgrowths. This information will help determine the timing of cementation and the source of the fluids that carried silica into the formation. Analysis of the carbon and oxygen isotopic composition of the carbonate cements should contribute information on the relative timing of the late-stage cements compared to the migration of hydrocarbons into the formation. Microprobe analysis of the composition of the carbonate cements may also provide information about the chemical conditions in the Travis Peak during burial diagenesis.

The goal of all these geochemical studies is to provide additional information about the processes that were operating in the Travis Peak during burial and which resulted in the drastic reduction of permeability in these sandstones. The initial petrographic studies have identified significant geographic and stratigraphic variations in cementation, porosity, and permeability in Travis Peak sandstones. An understanding of the processes that caused the cementation should provide insight into the causes of these regional variations in the

physical properties of the Travis Peak sandstones. All studies will provide further insight into the evolution of the low-permeability reservoir framework and into the origin and emplacement of the gas resource. This insight is necessary for effective reservoir exploitation and for development of new concepts of exploration and field delineation.

ACKNOWLEDGMENTS

This work was prepared for, and funded by, the Gas Research Institute under Contract No. 5082-211-0708, Robert J. Finley, Principal Investigator.

The cooperation of the following companies and operators is gratefully acknowledged: Amoco Production Company (USA), ARCO Oil and Gas Company, Ashland Exploration, Inc., Delta Drilling Company, Prairie Producing Company, Stallworth Oil and Gas, Inc., Sun Oil Company, and Clayton W. Williams, Jr.

Routine and special core analyses of samples from GRI cooperative wells were performed by Petrophysical Services, Inc. Elemental analysis of reservoir bitumen was conducted by Robertson Research (U.S.), Inc.

This manuscript was word processed by Dorothy C. Johnson under the direction of Lucille C. Harrell. Illustrations were prepared by Jana Brod, Tom Byrd, and Joel L. Lardon under the direction of Richard L. Dillon. Text illustration camerawork was by James A. Morgan. The manuscript was reviewed by Robert J. Finley and Edward C. Bingler. Technical editorial review was by Jules R. DuBar; editing was by Mary Ellen Johansen.

REFERENCES

David K. Davies and Associates, Inc., 1984a, Fluid sensitivity evaluation, Travis Peak sand zones, Sam Hughes No. 1 well, Panola County, Texas: Kingwood, Texas, report prepared for Petrophysical Services, Inc., 50 p.

_____1984b, Sensitivity evaluation of the 8,188 to 8,394.9 foot Travis Peak interval, ARCO B. F. Phillips No. 1 well, Smith County, Texas: Kingwood, Texas, report prepared for Petrophysical Services, Inc., 60 p.

_____1985a, Fluid sensitivity evaluation, three Travis Peak sand zones, Ashland S.F.O.T. No. 1 well, Nacogdoches County, Texas: Kingwood, Texas, report prepared for Petrophysical Services, Inc., 52 p.

_____1985b, Fluid sensitivity evaluation, three Travis Peak sand zones, Prairie Producing Mast No. A-1 well, Nacogdoches County, Texas: Kingwood, Texas, report prepared for Petrophysical Services, Inc., 64 p.

Finley, R. J., 1985, Chapel Hill field, in Finley, R. J., Dutton, S. P., Lin, L. S., and Saucier, A. E., The Travis Peak (Hosston) Formation: geologic framework, core studies, and engineering field analysis: The University of Texas at Austin, Bureau of Economic Geology, topical report prepared for Gas Research Institute under contract no. 5082-211-0708, p. 188-207.

Folk, R. L., 1974, Petrology of sedimentary rocks: Austin, Texas, Hemphill, 182 p.

Gold, P. B., 1984, Diagenesis of middle and upper Miocene sandstones, Louisiana Gulf Coast: The University of Texas at Austin, Master's thesis, 159 p.

Jonas, E. C., and McBride, E. F., 1977, Diagenesis of sandstone and shale: application to exploration for hydrocarbons: The University of Texas at Austin, Department of Geological Sciences Continuing Education Publication No. 1, 120 p.

Kreitler, C. W., Collins, E. W., Fogg, G. E., Jackson, M. P. A., and Seni, S. J., 1983, Hydrogeologic characterization of the saline aquifers, East Texas Basin--

implications to nuclear waste storage in East Texas salt domes: The University of Texas at Austin, Bureau of Economic Geology, draft report prepared for U.S. Department of Energy under contract No. DE-AC97-80ET46617, 55 p.

Rogers, M. A., McAlary, J. D., and Bailey, N. J. L., 1974, Significance of reservoir bitumens to thermal-maturation studies, western Canada Basin: American Association of Petroleum Geologists Bulletin, v. 58, no. 9, p. 1806-1824.

Saucier, A. E., 1985, Geologic framework of the Travis Peak (Hosston) Formation of East Texas and North Louisiana, in Finley, R. J., Dutton, S. P., Lin, Z. S., and Saucier, A. E., The Travis Peak (Hosston) Formation: geologic framework, core studies, and engineering field analysis: The University of Texas at Austin, Bureau of Economic Geology, topical report prepared for Gas Research Institute under contract no. 5082-211-0708, p. 3-74.

Saucier, A. E., Finley, R. J., and Dutton, S. P., 1985, The Travis Peak (Hosston) Formation of East Texas and North Louisiana: Proceedings, 1985 Society of Petroleum Engineers/Department of Energy Joint Symposium on Low Permeability Reservoirs, Denver, Colorado, SPE/DOE Paper No. 13850, p. 15-22.

Surdam, R. C., Boese, S. W., and Crossey, L. J., 1984, The chemistry of secondary porosity, in Clastic diagenesis: American Association of Petroleum Geologists Memoir 37, p. 127-149.

Tissot, B. P., and Welte, D. H., 1978, Petroleum formation and occurrence: New York, Springer-Verlag, 538 p.

Wilson, M. D., and Pittman, E. D., 1977, Authigenic clays in sandstones: recognition and influence on reservoir properties and paleoenvironmental analysis: Journal of Sedimentary Petrology, v. 47, no. 1, p. 3-31.

Plate I.

A. Photomicrograph of quartzarenite from a depth of 9,959.9 ft in the Prairie #1-A Mast core. Primary pores have been almost completely occluded by interlocking quartz cement. Long dimension of photo = 2.6 mm; crossed-polarized light.

B. Secondary porosity (P) within plagioclase feldspar from a depth of 10,112.4 ft in the Ashland #1 S.F.O.T. core. Long dimension of photo = 0.26 mm; plane-polarized light.

C. Photomicrograph of primary (PP) and secondary (SP) pores and euhedral quartz overgrowths (Q) from a depth of 6,843.7 ft in the Clayton Williams #1 Sam Hughes core. Long dimension of photo = 0.26 mm; plane-polarized light.

D. Photomicrograph of elongate primary pores (P) between quartz overgrowths. Ankerite cement is dark material at the left. Depth is 9,161.0 ft in the Prairie #1-A Mast core. Long dimension of photo = 0.65 mm; plane-polarized light.

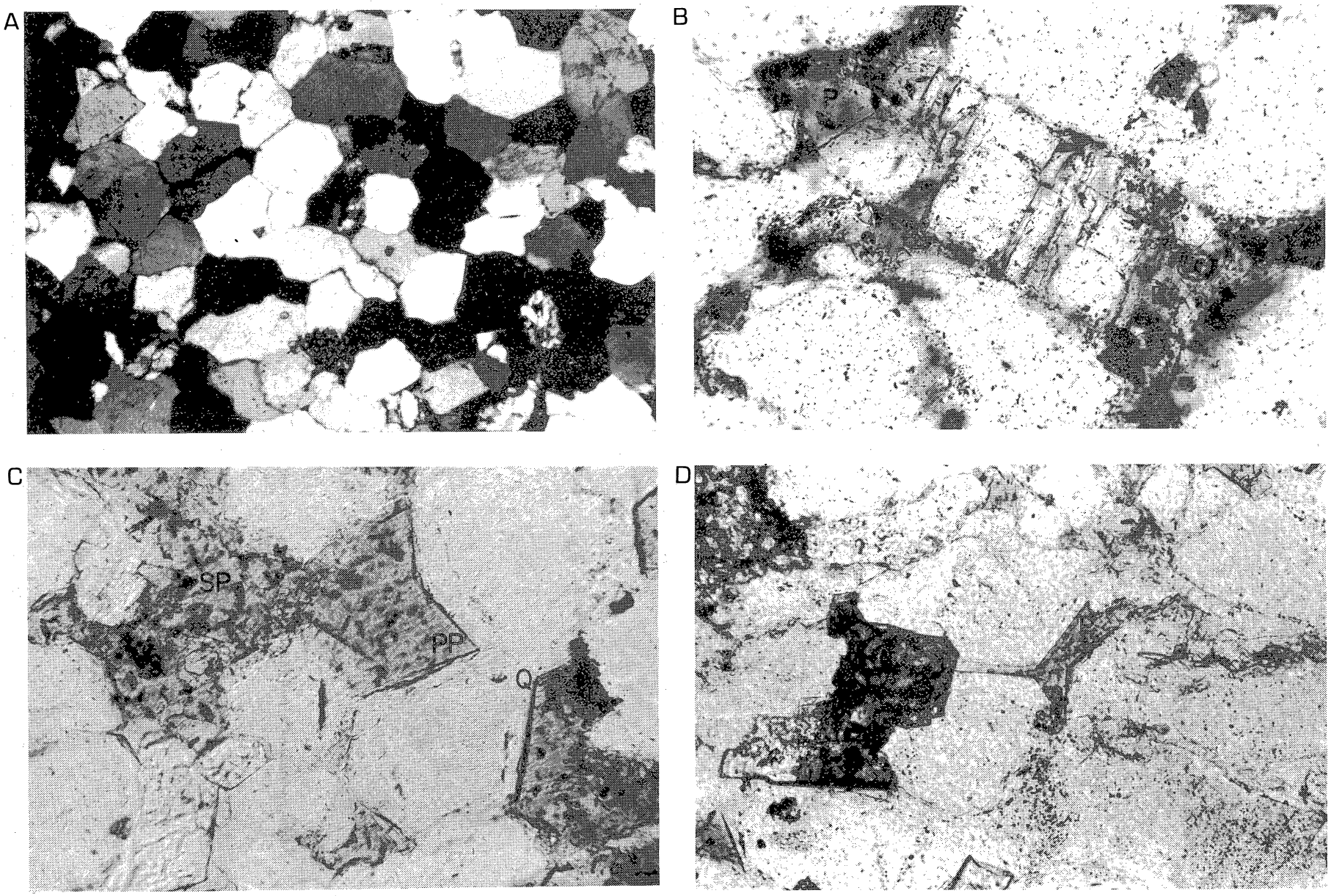
A
B
P
C
SP
PP
Q
D

Plate II.

A. Photomicrograph of abundant chlorite cement (C) within a secondary pore from a depth of 8,639.1 ft in the Prairie #1-A Mast core. Long dimension of photo = 0.26 mm; plane-polarized light.

B. Dolomite cement (D) with increasing iron content toward the crystal edges, where the composition is ankerite (A). Depth is 9,753.6 ft in the Ashland #1 S.F.O.T. core. Long dimension of photo = 0.26 mm; plane-polarized light.

C. Ankerite cement (A) precipitated after quartz overgrowths (Q) at a depth of 8,669.0 ft in the Prairie #1-A Mast core. Long dimension of photo = 0.26 mm; plane-polarized light.

D. Dolomite and ankerite cement (C) concentrated along a ripple face at a depth of 9,753.0 ft in the Ashland #1 S.F.O.T. core. Long dimension of photo = 2.6 mm; plane-polarized light.

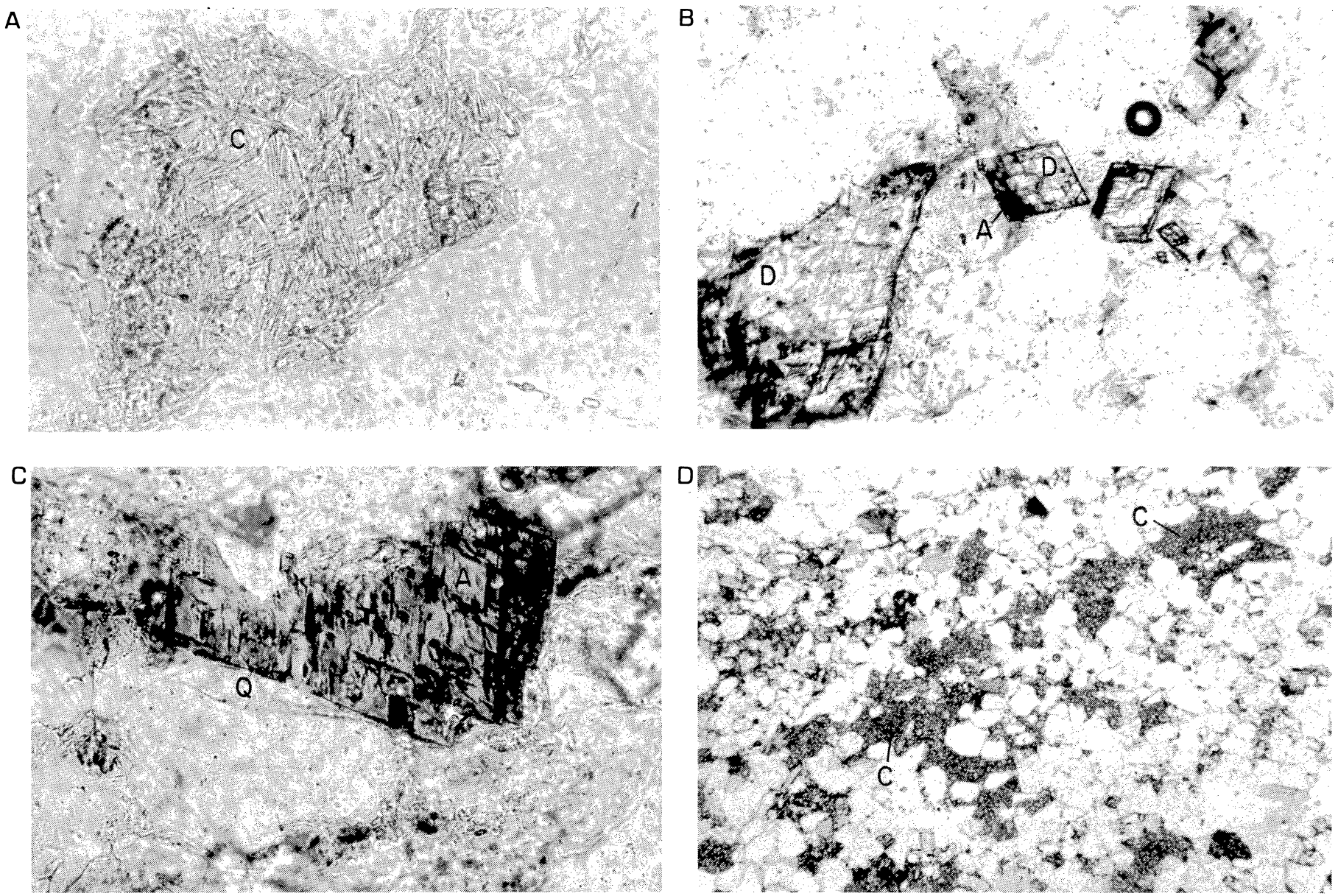
A
C
B
D
A
D
C
Q
A
D
C
C

Plate III.

A. Anhydrite cement (AN) occluded porosity and replaced framework grains and cements at a depth of 9,154.9 ft in the Prairie #1-A Mast core. Long dimension of photo = 0.65 mm; crossed-polarized light.

B. Pyrite (black) replaced both detrital grains and quartz cement at a depth of 9,991.1 ft in the Prairie #1-A Mast core. Long dimension of photo = 2.6 mm; plane-polarized light.

C. Reservoir bitumen (dark areas) in primary porosity at a depth of 8,386.7 ft in the ARCO #1 B. F. Phillips core. The reservoir bitumen was emplaced after precipitation of quartz overgrowths. Long dimension of photo = 0.89 mm; plane-polarized light.

D. Reservoir bitumen (dark areas) entered pores after the precipitation of quartz overgrowths (Q). Depth is 8,386.7 ft in the ARCO #1 B. F. Phillips core. Long dimension of photo = 0.35 mm; plane-polarized light.

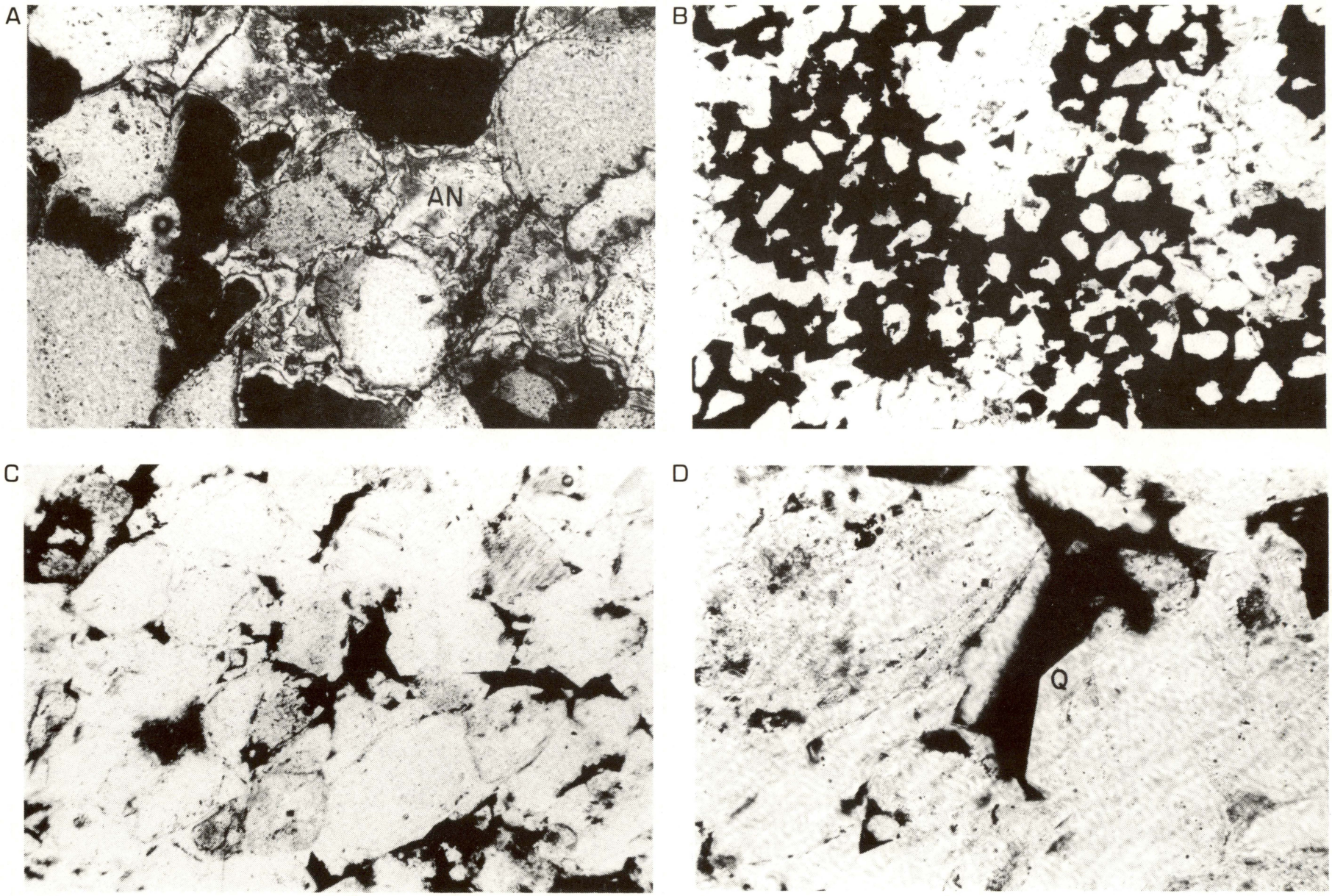
A
AN
B
C
D
Q

Plate IV.

A. SEM photograph of abundant quartz overgrowths (Q). Primary pores are elongate slits (arrow) between quartz overgrowths. Depth is 9,226.7 ft in the Prairie #1-A Mast core. Bar length is 100µm; magnification is 200x.

B. SEM photograph of euhedral quartz overgrowths (Q) in a sample that retains 12 percent porosity. Depth is 8,246.1 ft in the ARCO #1 B. F. Phillips core. Bar length is 100 µm; magnification is 200x.

C. SEM photographs of pore-lining illite (I) and chlorite (C). Abundant microporosity occurs between clay crystals. Depth is 9,753.6 ft in the Ashland #1 S.F.O.T. core. Bar length is 10 µm; magnification is 3500x.

D. SEM photograph of authigenic chlorite (C) in a secondary pore. Depth is 8,246.1 ft in the ARCO # 1 B. F. Phillips core. Bar length is 10 µm; magnification is 1500x.

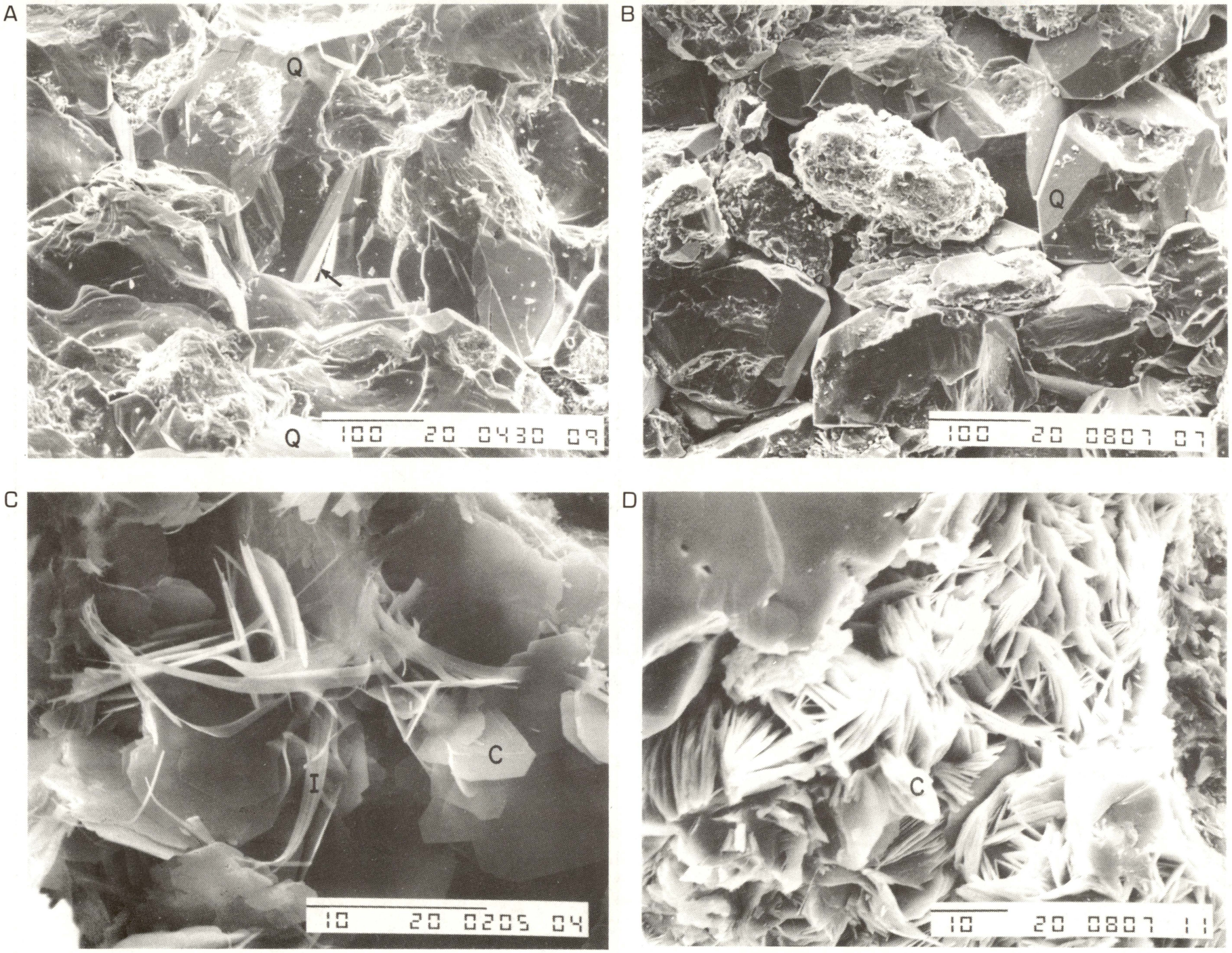
A
Q
Q
100 20 0430 09
B
Q
100 20 0807 07
C
I
C
10 20 0205 04
D
C
10 20 0807 11

Plate V.

A. SEM photograph of an illite rim (I) around a detrital grain, which prevented precipitation of quartz overgrowths except where there were breaks in the illite. Depth is 8,246.1 ft in the ARCO #1 B. F. Phillips core. Bar length is 100 µm; magnification is 500x.

B. SEM photograph of illite fibers (I) within secondary porosity in a leached plagioclase (P). Depth is 8,178.7 ft in the Stallworth #2-B Everett core. Bar length is 10 µm; magnification is 2000x.

C. SEM photograph of an ankerite rhomb at a depth of 9,753.6 ft in the Ashland #1 S.F.O.T. core. Bar length is 10 µm; magnification is 1500x.

D. SEM photograph of a leached plagioclase grain with internal albite overgrowths (A) from a depth of 8,246.1 ft in the ARCO #1 B. F. Phillips core. Bar length is 100 µm; magnification is 500x.

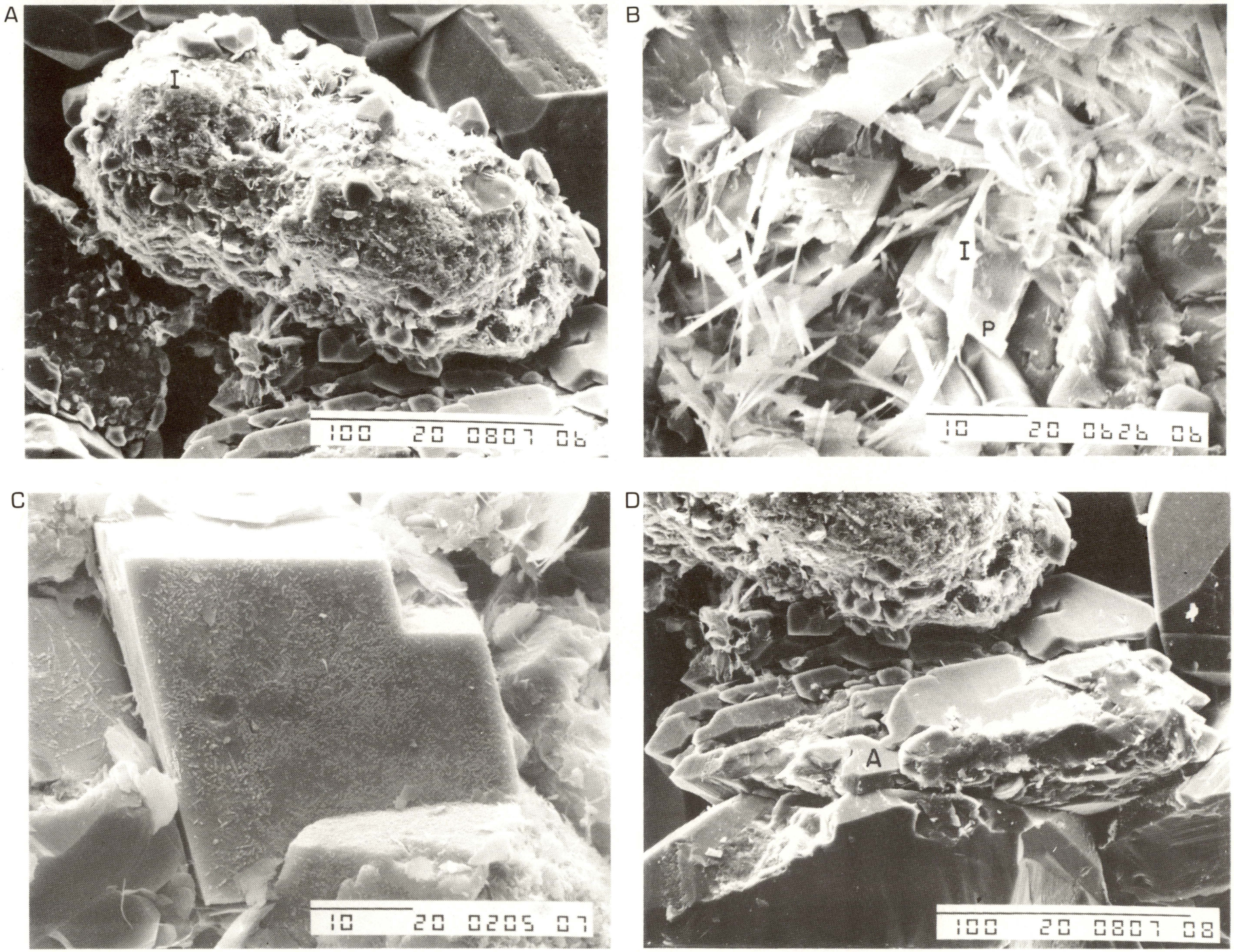
A
I
100 20 0807 06
B
I
P
10 20 0626 06
C
10 20 0205 07
D
A
100 20 0807 08